

Dielectric Barrier Discharge (DBD) Plasma Coating of Sulfur for
Mitigation of Capacity Fade in Lithium-Sulfur Batteries

Peer-reviewed author version

SHAFIQUE, Ahmed; Rangasamy, VS; Vanhulsel, A; SAFARI, Momo; Gross, S;
ADRIAENSENS, Peter; VAN BAEL, Marlies; HARDY, An & Sallard, S (2021)
Dielectric Barrier Discharge (DBD) Plasma Coating of Sulfur for Mitigation of
Capacity Fade in Lithium-Sulfur Batteries. In: ACS Applied Materials & Interfaces, 13
(24) , p. 28072 -28089.

DOI: 10.1021/acsami.1c04069

Handle: <http://hdl.handle.net/1942/35895>

Dielectric barrier discharge (DBD) plasma coating of sulfur for mitigation of capacity fade in lithium-sulfur batteries.

*Ahmed Shafique, ^{a,b,d} Vijay Shankar Rangasamy, ^{a,d} Annick Vanhulsel, ^{a,d} Mohammadhosein Safari, ^{b,c,d} Silvia Gross, ^e Peter Adriaensens, ^{b,c} Marlies K. Van Bael, ^{b,c,d} An Hardy, ^{*b,c,d} Sébastien Sallard ^{*a,d}*

^a. VITO (Flemish Institute for Technological Research), Sustainable Materials, 2400 Mol, Belgium.

^b. Hasselt University, Institute for Materials Research (imo-imomec), Martelarenlaan 42, B 3500 Hasselt Belgium.

^c. Imec vzw, div. imomec, Wetenschapspark 1, B 2590 Diepenbeek, Belgium.

^d. Energyville, Thor Park 8320, B-3600 Genk, Belgium.

^e. University of Padua, Department of Chemical Sciences, via Marzolo, 1, 35131 Padova PD, Italy.

KEYWORDS

Lithium-sulfur, Battery, Surface coating, Plasma, Dielectric barrier discharge, Aging.

ABSTRACT

Sulfur particles with a conductive polymer coating of poly(3,4-ethylene dioxythiophene) “PEDOT” were prepared by dielectric barrier discharge (DBD) plasma technology under atmospheric conditions (low temperature, ambient pressure). We report a solvent free, low cost, low energy consumption, safe, and low risk process to make the material development and production compatible for sustainable technologies. Different coating protocols were developed to produce PEDOT-coated sulfur powders with electrical conductivity in the range of 10^{-8} - 10^{-5} S/cm. The raw sulfur powder (used as reference) and (low-, optimum-, high-) PEDOT-coated sulfur powders were used to assemble lithium-sulfur (Li-S) cells with high sulfur loading of ~ 4.5 mg/cm². Long-term galvanostatic cycling at C/10 for 100 cycles showed that the capacity fade was mitigated by $\sim 30\%$ for the cells containing the optimum-PEDOT coated sulfur in comparison to the references Li-S cells with raw sulfur. Rate capability, cyclic voltammetry, and electrochemical impedance analyses confirmed the improved behavior of the PEDOT coated sulfur as an active material for lithium-sulfur batteries. The Li-S cells containing optimum-PEDOT coated sulfur showed the highest reproducibility of their electrochemical properties. A wide variety of bulk and surface characterization methods including conductivity analysis, X-ray diffraction (XRD), scanning electron microscope (SEM), Raman spectroscopy, X-ray photoelectron spectroscopy (XPS), and nuclear magnetic resonance spectroscopy (NMR) were used to explain the chemical features and the superior behaviour of Li-S cells using the optimum-PEDOT coated sulfur material. Moreover, post-mortem (SEM and BET) analyses of uncoated and coated samples allow us to exclude any significant effect at electrode scale even after 70 cycles.

1.0 Introduction

Ecological concerns related to the massive use of fossil fuels (e.g. global warming) are well known and widely accepted today. For this reason, one of the primary technological challenges of this century is to increase the production and storage of renewable energy/electricity.¹

The demand for energy storage has dramatically increased in the two last decades, especially in the case of electrical energy storage in batteries.² Since their first commercialization in 1991, lithium-ion (Li-ion) batteries are one of the most attractive solutions for energy storage applications. In particular, their long lifespan, flexible lightweight design, specific power, and specific energy value make Li-ion batteries a suitable candidate for transport applications.³ Currently, Li-ion batteries are mainly based on lithium metal oxides (LiCoO_2 , $\text{LiNi}_x\text{Mn}_y\text{Co}_z\text{O}_2$, and LiMn_2O_4) or phosphates (LiFePO_4) and carbon systems with theoretical specific energy in the range of 150–260 Wh/kg.^{4,5} From the sustainability point of view, it is important to reduce or eliminate the presence of cobalt (Co) in the positive electrode because it is an expensive and critical raw material. The increasing interest in electric vehicles and hybrid electric vehicles pushes the research towards new active materials with higher performances (mainly higher energy) and lower prices.^{6,7,8} In addition, the current processing of Li-ion battery positive electrodes is based on PVDF (binder) and NMP (solvent). Thus, this technology can hardly be considered to be sustainable.⁹ Due to the massive increase in battery demand and production, the sustainability of the battery manufacturing is already gaining significant attention.^{10,11}

Therefore, new lighter weight, low-cost materials must be scouted in order to meet the high specific energy needed for modern technology applications.¹² Among different candidates, sulfur seems one of the most promising challengers to the Li-ion batteries due to the high theoretical specific capacity of 1675 mAh/g of the sulfur following the theoretical reaction $\text{S} + 2 \text{e}^- + 2 \text{Li}^+ \rightarrow$

Li₂S. Besides, sulfur is an abundant, lightweight, and non-toxic element with a low environmental footprint, which eventually decreases the final cost and makes the battery more sustainable.¹³ Nevertheless, due to the sulfur present in the positive electrode, lithium-sulfur (Li-S) batteries suffer from various challenges that hinder their commercialization. It is well known that sulfur particles suffer from the problems of poor electronic conductivity ($\sim 5 \times 10^{-30}$ S/cm at 25 °C), large volume expansion ($\sim 80\%$) during cycling, and dissolution of intermediate polysulfides into the electrolyte by the polysulfide shuttle effect, which eventually leads to low coulombic efficiency and rapid capacity decay on cell level.^{14,15,16}

In the last ten years, vast research efforts have been invested in the field of Li-S batteries, which has led to remarkable advances compared to the earliest configuration, but still, the actual technology of the Li-S batteries is far from having reached its full potential.^{12,13,14} The four main components (positive electrode, negative electrode, separator, and electrolyte) must be designed with an integrated approach that focuses on high energy density, high efficiency, fast charging, and improved cycling stability.

The development of advanced sulfur powder and sulfur electrodes is focusing on increasing the stability of the specific capacity and the rate capability. The pioneering work of Nazar et al.¹⁷ reported the idea of trapping sulfur in a mesoporous carbon matrix. The motivation behind this work was to **ensure** better electronic accessibility of the sulfur (nano-sized and within a conductive matrix) and trapping it in the matrix. In addition, other methods have been developed by using mesoporous TiO₂ nanotubes¹⁸, mesoporous carbon spheres¹⁹, sulfur-wrapped in graphene²⁰, embedded in reduced graphene oxide (rGO)²¹ following a similar trend (trapping sulfur). The standard method to insert the sulfur in a porous rigid-host is the melting approach using the low melting point of sulfur and capillary adsorption as a driving force. Other strategies to improve the

life cycle involve optimizing the liquid electrolyte composition by using additives ^{14,22} or using a solid-state polymer electrolyte ^{16,23} or by setting an appropriate electrolyte/sulfur ratio. ^{15,24}

Impressive progress has been made during the last ten years, especially by focusing on the development of sulfur positive electrodes. ^{2,12} Upon cycling, the morphology of the positive electrode changes significantly. When the battery operation starts, the active material leaves the carbon/binder matrix and dissolves in the electrolyte in the form of soluble polysulfides. This eventually affects the overall porosity of the electrode and may give rise to collapse and strong electrode pulverization. Reprecipitation (Li_2S or S_8 on (dis)charge) is usually heterogeneous, leading to the formation of **large** particles that are mostly inactive, due to the poor conductivity of the solid products, and increase the mechanical stress in the positive electrode. Also, the current collector may get disconnected from some parts of the carbon/binder agglomerates, resulting in loss of active surface area which eventually leads to drastic capacity fading right after the initial cycles. ¹⁶ In general, to decrease the capacity fading, the positive electrode should retain its morphology over the number of cycles. Thus, not only the sulfur trapping, but also the entire structure of the sulfur positive electrode is important. ^{25,26,27,28}

In recent times, surface coating is considered to be an effective method for improving the electrochemical performances of positive electrode materials. Carbon is an ideal coating material due to its high electrical conductivity, elastic nature, and dense structure. Carbon coating has been successfully used to enhance the properties of various electrode materials. ^{12,29} However, to increase the electronic conductivity of the coating layer traditional techniques for carbon coating, like hydrothermal ³⁰ and CVD (chemical vapor deposition) ³¹ mostly require thermal treatment at high temperature ($>500\text{ }^\circ\text{C}$), which is not suitable for sulfur. In addition, due to the limited porosity

of carbon matrix, the sulfur content in the electrode is limited at 50% weight ratio and leads to limited energy density of the Li-S batteries.¹³

Furthermore, to modify the sulfur-based negative electrode, intrinsically polar metal oxides (such as ZrO_2 ,³² MoO_2 ,³³ MgO ,³⁴ CeO_2 ,³⁴ CaO ,³⁴ Fe_2O_3 ,³⁵ etc) have been widely used in Li-S batteries. These metal oxides can interact as polar lithium polysulfide trappers. Metal oxide (like Al_2O_3) coating using atomic layer deposition (ALD) can also be considered as the state of the art.^{36,37,38,39} To the best of our knowledge, no direct coating of sulfur particles by ALD was ever reported, as multiple steps and complex processes are required for the use of ALD in Li-S batteries. Kim et al.³⁸ and Yu et al.³⁹ reported the prolonged cycle life of Li-S batteries using ALD. Kim et al. showed that alumina coating on the carbon sphere impregnated with sulfur limits the sulfur deposition during cycling on the Li-negative electrode. However, the alumina coated electrodes show significant capacity fading after several cycles. The authors attributed it to the resistance build-up on the Li negative electrode (anode). One has also to consider the leaching of metal oxide on long term during the lifetime of the batteries by the HF present in the electrolyte, especially for amorphous coating as formed by ALD. A shuttling phenomena to the negative electrode is probably occurring with the formation of metallic nanoparticles on the electrode surface that may act as electrocatalysts promoting the degradation of the electrolyte.⁴⁰

Many research groups reported on the positive impact of coating sulfur particles with conducting polymers.^{41,42} Such conducting polymers allow an increase in the electronic conductivity at the surface of the sulfur particles. Thus, similar to the carbon coating of LiFePO_4 in Li-ion batteries, electronic percolation is increased within the sulfur electrode of Li-S batteries, even if the bulk of the active material (sulfur) itself remains poorly conductive. In addition, the polymeric coating (in certain cases) acts as a barrier to mitigate the polysulfide shuttle phenomenon. Consequently, the

electrochemical performance of the Li-S cell in terms of capacity, charge/discharge rate, and ageing is reported to be significantly improved.^{43,44}

Among the different conducting polymers, the most promising one is poly-3,4 ethylene dioxythiophene, commonly labelled as PEDOT. Li et al.²⁶ reported a PEDOT coating having a superior effect to polypyrrole (PPy) and poly-aniline (PANI) coatings because PEDOT was found to hinder the polysulfide shuttle by favorable chemical interactions (chemical trapper) with the polysulfide (Li_2S_8 - Li_2S). Hence, besides increasing the conductivity of the sulfur electrode and in addition to its barrier properties as a membrane, PEDOT acts as a chemical trapper, even after 300 cycles. Most of these publications^{41,42,44,45} report similar improvements i.e. higher and more stable specific capacity, improved rate capability compared to non-modified sulfur powder

Nevertheless, the main drawback of all the above-mentioned approaches is that they do not appear to be compatible with up-scaling. They include complex time-consuming steps for solvent removal and are limited to small batches and laboratory-scale production. Many synthetic methods reported are multi-step and complex, they may need the use of autoclaves^{16,18,46} or sealed-glass tubes⁴⁷ or require the use of hazardous chemicals like HF^{16,48} or high-power centrifugation.^{25,26,49,50,51,52}

Recently, the surface modification of flat surfaces (with the deposition of a conductive PEDOT-thin film) was reported by polymerization of the 3,4 ethylene dioxythiophene (EDOT) under dielectric barrier discharge (DBD) plasma treatment.⁵³ In the current paper, we report an alternative new approach (powder functionalization) for coating commercial sulfur powder with PEDOT by means of a dry coating route, based on DBD-technology. Advantages are that the DBD plasma device operates at low temperature and ambient pressure conditions and does not require high energy. Moreover, it is a dry method (no solvent chemicals, and limited amount of precursors) that does not require energy-intensive drying steps that might lead to aggregation. Thus, the DBD-

plasma process is compatible with the sulfur element and entails low cost, low energy consumption, and low safety risk. All these factors make the coating of sulfur particles with the DBD-plasma technology compatible with up-scaling and sustainability.⁵⁴ Moreover, the sulfur electrodes can be processed by a water-based protocol which is more environmental friendly and requires less energy during the solvent removal than the conventional method using NMP.

The materials were intensively characterized to correlate the effect of the PEDOT-coating on the electrochemical properties of the Li-S cells using raw and (low-, optimum-, high-) PEDOT-coated sulfur powders as active materials in the positive electrodes. In addition, the electronic conductivity of the PEDOT coated powders is stable after more than six months. Post-mortem analyses on cycled electrodes (SEM and BET) were performed to confirm that the difference observed in the performance of the Li-S cells using different sulfur materials (raw or PEDOT-coated) could not be influenced by any significant macroscopic (electrode scale) phenomena.

2.0 Experimental part

2.1: Materials:

The sulfur powder (Merck, 99-101%) was sieved at 50 μm before use. The carbon black (Imerys Graphite & Carbon) powder C-nergy Super-C65, was sieved at 125 μm . EDOT monomer was purchased from TCI (> 98 %). Lithium polyacrylate (LiPAA) was obtained by neutralization of polyacrylic acid aqueous solution (Sigma-Aldrich, 35% weight with $M_w \sim 250\,000$) to $\text{pH} \sim 8.1$ with LiOH aqueous solution ($C \sim 2\text{mol/L}$) with the final content of the LiPAA aqueous solution was 10% in weight, adjusted by the addition of deionized water as previously reported.⁵⁵

2.2: Materials synthesis (surface coating by DBD-plasma process)

An atmospheric plasma process was developed (Figure 1) that enables to coat sulfur particles with a plasma polymerized PEDOT coating. The atmospheric plasma device is a cylindrical dielectric barrier discharge (DBD) configuration designed to treat powders under atmospheric conditions (low temperature $\ll 100^\circ\text{C}$, ambient pressure, and solvent free). The system consists of a glass tube, which in its center contains a metal electrode that is grounded. The cylinder ratio thus is equivalent to the plasma gap, which is 2 mm. Surrounding the external perimeter of the glass tube there is a metal mesh connected to a high voltage power supply. An AC-power supply (AFS-GmbH) and transformer are used to ignite the plasma. The reported frequency and power are the properties of the signal delivered from the generator. Sulfur powder is injected with the plasma gas (argon) using a powder feeder pump (IMPAKTTM). The EDOT precursor is introduced in the plasma as an aerosol. After plasma treatment, the plasma gas is evacuated through a filter and the treated powder is collected from the bottom. This process can be repeated several times in order to increase the residence time of the sulfur particles in the plasma, which eventually increases the coating thickness on the powder surface.^{56,57,58} The plasma treatments were done at 500W plasma

power and a frequency of 18kHz. The Ar gas flow was set at 30 slm with addition of 1.5 slm O₂ (which acts as an oxidizing dopant to control the polymer oxidation) and the total processing time was fixed at 55 minutes. However, the precursor injection dose was varied from 30 mg/min, 75 mg/min, and 100 mg/min. This way the so-called low, optimum, and high PEDOT samples were obtained respectively.

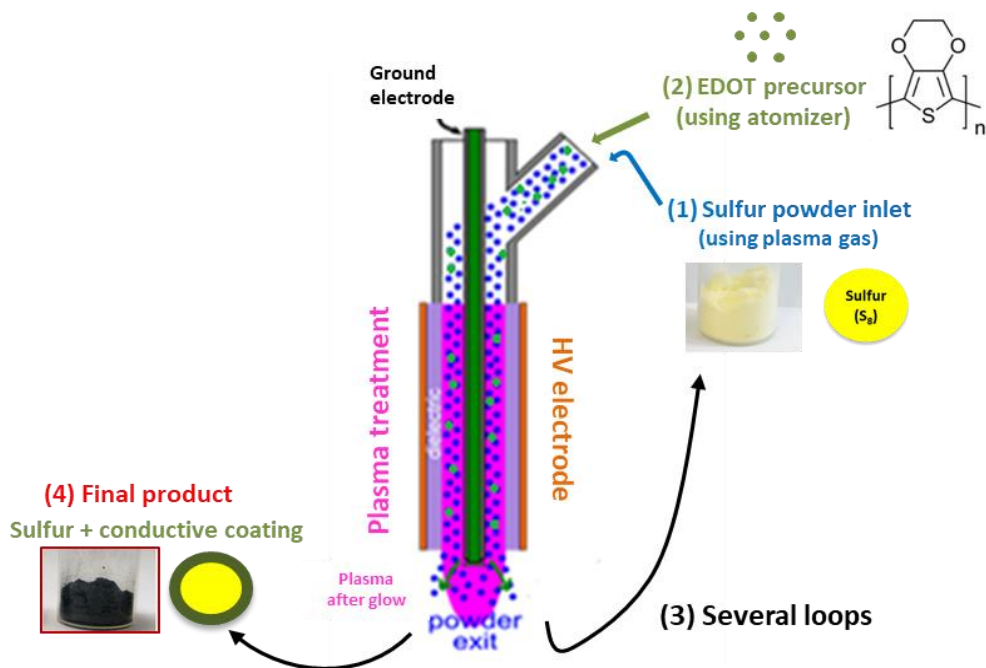


Figure 1: Schematic sketch of the atmospheric plasma process for surface modification of sulfur powder.

Table 1 summarizes the process conditions to synthesize the PEDOT-coated sulfur powders that have been studied in this work. The presence of O₂ is needed in the argon atmosphere with an optimum of 5% to get measurable electronic conductivities ($> 10^{-11}$ S/cm). As it is expected from a π conjugated polymer, the oxidation state of the PEDOT influences dramatically its conductivity. Similarly, as the plasma power can be varied, low power leads to less EDOT activation and consequently less polymerization, resulting in a very thin coating. In addition, power superior to 500 W leads either to no significant improvement of the conductivity of the final product or drop

of the measured conductivity, or even a complete degradation of the sulfur powder (PEDOT inactivation and/or sulfur sublimation) when reaching 800 W.

Table 1: Experimental conditions for the reported DBD-plasma coated sulfur powders.

Sample	Amount of (PEDOT) precursor	Plasma power	Frequency	Plasma feed gas (Ar)	Change in additive gas O ₂	Process time
	(mg/min)	(W)	(KHz)	(slm)	(slm)	(min)
Raw sulfur	0	500	18	30	1.5	55
Low- PEDOT	30					
Optimum- PEDOT	75					
High- PEDOT	100					

2.3: Characterization techniques

Conductivity: The powder conductivity is measured (Figure S1) by a home-made device connected to a digital precision multimeter (DMM-4050, Tektronix). A detailed description of conductivity measurements is reported in the supporting information.

Laser diffraction: The particle size dispersion (PDS) of the different sulfur powders were measured using a Microtrac S3500 particle size analyser.

XRD: X-ray diffraction (XRD, Empyrean) patterns were recorded using monochromatic Co-K α radiation at 45 kV and 40 mA, to study the structural phases in each sample. The diffraction patterns were recorded with 2D-detector at a scan speed of 0.067335° /sec between 10° and 90°.

SEM: The particle morphologies for raw and coated sulfur powders were characterized by scanning electron microscope (SEM) from FETTM NovaSEM 450 using backscattered electron images taken using a CBS detector and an acceleration voltage of 5 kV, with all the measurements were performed in a vacuum chamber (pressure: 10⁻⁶ mbar).

TEM: We used FEI Tecnai G2 Spirit Twin, at 120 kV. Samples were dispersed in absolute ethanol, sonicated for ~30 seconds, dropped onto carbon-coated copper grids (EMS, FCF-200-Cu), and dried under an infrared lamp for several minutes.

XPS: Samples were investigated by XPS measurements with a Φ 5600ci Perkin-Elmer spectrometer, using a standard aluminum (Al K α) source with an energy of 1486.6 eV operating at 220 W.

Raman: The Raman spectra were collected on a Horiba Jobin Yvon T64000 triple Raman spectrometer. A BXFM Olympus microscope (100x magnification objective), a Horiba Jobin Yvon Symphony CCD detector, and a 488 nm Lexel SHG laser operated at less than 20 mW were used.

NMR: The ^{13}C NMR spectra (CP/MAS) were recorded at room temperature on a Jeol ECZ600R 600MHz spectrometer (14.1 T wide-bore magnet) equipped with a 3.2 mm wide VT Range HXMAS probe.

2.4: Electrode preparation

Raw and PEDOT coated sulfur-based electrodes were prepared with an established protocol.⁵⁵ Typically, a tape casting method by mixing sulfur: carbon-black: binder (LiPAA) with a composition of 66:24:10 in weight ratio using mechanical stirring at 650 rpm for 15 mins. The liquid/solid ratio in LiPAA polymeric binder solution was adjusted by mixing the LiPAA (10% weight) aqueous solution with water to reach 2% LiPAA in weight. Ethanol (VWR, 96% denatured with 3% isopropanol) was added afterward (with a 3:2 wt.% ratio compared to LiPAA solution, respectively). An additional amount of acetone (ratio of LiPAA/acetone is 1:1 by weight respectively) was added into the dispersion. The slurries were coated on carbon-coated aluminum-foil (Al/C) (MTI-KJ group, thickness 16 μm) by doctor-blading, and dried in a fume-hood at room

temperature. The electrodes were punched, weighed, and dried overnight in a desiccator and then placed in the transfer chamber under vacuum for 15 min before entering the glove box. The average sulfur loading was calculated to be $\sim 4.5 \text{ mg/cm}^2$ for all electrodes.

2.5: Battery assembly and testing

Coin cells (CR2032) were assembled in an argon filled glove box (Jacomex GP-concept) with $\text{H}_2\text{O} < 1 \text{ ppm}$ and $\text{O}_2 < 1 \text{ ppm}$ with sulfur positive electrodes (area: 1.77 cm^2 , diameter: 15 mm) and a disc of lithium metal (Alfa Aesar 99.9%) of 16 mm diameter as the negative electrode. A polymeric separator (Celgard 2400, diameter: 19 mm) was positioned between the two electrodes. Each cell was filled with 90 μL of electrolytic solution (SoulBrain MI), i.e. 1M lithium bis(trifluoromethanesulfonyl)imide (LiTFSI) in 1,3-dioxolane (DOL): dimethoxyethane (DME) with 1:2 as the weight ratio. LiNO_3 (Aldrich, 99.99% trace metal basis) was added to the electrolyte to reach 5% weight ratio. The cells were sealed with a pneumatic press in the glove-box and transferred in a temperature chamber at 25°C and connected to the battery tester (BCS-810 from Bio-Logic for galvanostatic cycling and Ametek PARSTAT PMC-1000 for impedance measurements). The coin cells were equilibrated for 6 hours at OCV and then cycled over a voltage range of 1.5 – 3.0 V vs. Li^+/Li . The cells were tested by different means, either at a single C-rate of C/10 for long cycling tests or different (dis)charge rates with C/10 for the first 30 cycles, followed by C/5, C/2, 1C, and C/10 rates with 10 cycles for each step. In the electrochemical impedance spectroscopy (EIS) tests, cells were left at OCV for 1 hour before the characterization. Cyclic voltammetry tests were performed from 1.0 – 3.0 V vs. Li^+/Li with scan rates of 0.1, 0.2, 0.5 and 2 mV/s. The scan rate of the linear sweep voltammetry (LSV) tests was 0.1 mV/s over a voltage range of 1.5 – 5.0 V vs. Li^+/Li . Post mortem SEM analysis of the electrodes was performed as reported in our previous article.⁵⁵

3.0: Results and Discussion

3.1: Characterization

A clear color difference was observed between the different sulfur powders before and after PEDOT coating (Figure 2). The commercial raw sulfur is golden yellow whereas low-, optimum- and high- PEDOT coated sulfur samples are light green, dark green, and black respectively. The difference in colorations can most probably be ascribed to the increase in the quantity of PEDOT present on the sulfur. The electronic conductivity of the raw sulfur could not be measured in our set-up, a value of $\sim 10^{-30}$ S/cm was taken from literature.⁴² However, the electronic conductivity is the highest for the optimum-PEDOT coated sulfur powder ($\sim 10^{-5}$ S/cm) followed by the high- and low- PEDOT coated sulfur powder ($\sim 10^{-6}$ and $\sim 10^{-8}$ S/cm), respectively. Because the measurement is not done on a single particle, grain boundary effects must be considered, and the result is considerably affected by the powder compressibility and the pressure applied. Therefore, the conductivity values have to be considered as semi-quantitative. In the present case, all measurements were done under the same conditions and repeated (see part 2.3 and supporting information). Abessolo et al.⁵³ obtained a conductivity of 10^{-2} S/cm for PEDOT films produced by DBD-plasma, which does not contradict with the lower values for the coated powders, due to possible grain boundaries effect. Consequently, and given a difference of at least one order of magnitude between the samples produced with the different protocols, the conductivity values and evolution are considered reliable.

The difference in the conductivity between the three PEDOT-coated samples will be affected/influenced at different levels: (i) at the molecular level, the regularity of the π - π conjugation will affect the electron mobility within a single chain of PEDOT; (ii) at the macroscopic level, the homogeneity and continuity of the PEDOT coverage of the sulfur particles

will determine the conductivity (mobility of electrons) between the different PEDOT chains and (iii) the grain boundaries might influence the inter-particle conductivity.

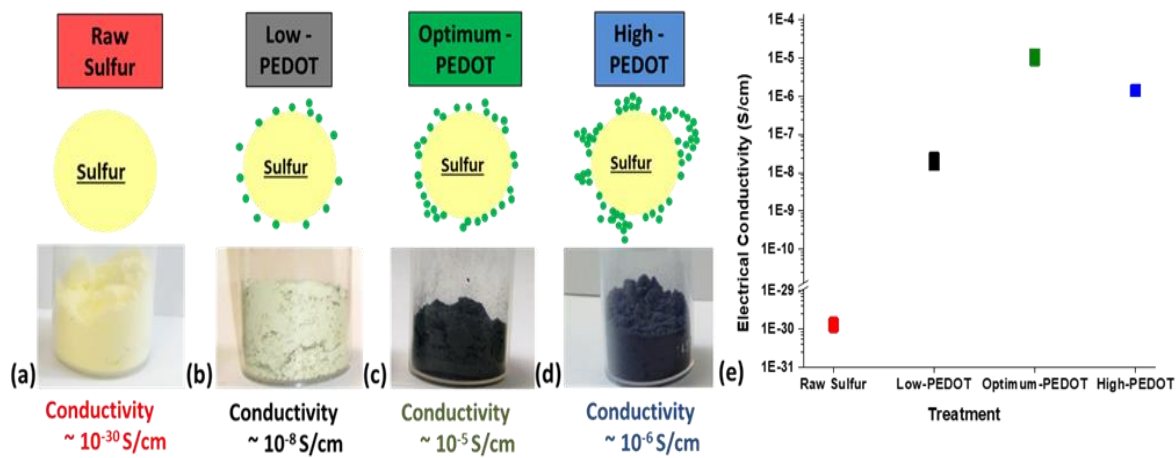


Figure 2: Selection of different coated and uncoated powders a) raw sulfur b) low- c) optimum- d) high-PEDOT and e) conductivity values.

The low conductivity of low-PEDOT coated sulfur powder is most probably attributed to the thin and incomplete coverage (as expected) due to the limited amount of precursor used in the coating protocol. The lower conductivity of the high-PEDOT coated sulfur vs. the optimum-PEDOT coated sulfur might be explained by two possible phenomena. As the high-PEDOT coated sulfur powder is highly wet just after the coating process, it is more likely that the polymerization of the EDOT precursor was not completed during the plasma-treatment. This effect is enhanced by the extensive amount of precursor used in the coating step, leading to more inhomogeneities both in (i) the π - π conjugation as suggested by Abessolo et al.⁵³ (see Figure 6 and related discussion on Raman-spectroscopy data) and (ii) coating morphology. Important to note is that the powder coating process is repeatable under the given experimental conditions and that the conductivity of the PEDOT-coated sulfur powders is stable at least for several months.

The cumulative particle size distribution (PSD) for uncoated and coated sulfur powders is quite similar (Figure S2). We observe a small increase in the average PSD of the PEDOT-coated sulfur

powders. This is attributed to limited (but still present) aggregation during the formation of the PEDOT-coating. We suppose during the coating initiation and growth, the latter is able to act as a glue for nearby sulfur particles. Based on the results we exclude any aggregation phenomena due to the plasma itself.

XRD analysis (Figure 3) provides details about the crystal structure of the uncoated and coated sulfur powders. The patterns of raw and PEDOT coated sulfur powders show distinguished (040) and (222) reflections around 32° and 26° , as well as smaller diffraction peaks, which fit JCPDS (no. 19-247) without any impurity phase. This indicates similar and conventional patterns of sulfur in its orthorhombic phase with the Fddz-space group.^{42,51} The PEDOT-coated sulfur powders present exactly the same diffraction pattern as the raw sulfur powder, thus indicating that the PEDOT coating is amorphous and/or too thin to be measurable in XRD. It also confirms that the DBD-plasma coating process does not alter the crystal structure of the sulfur material itself.

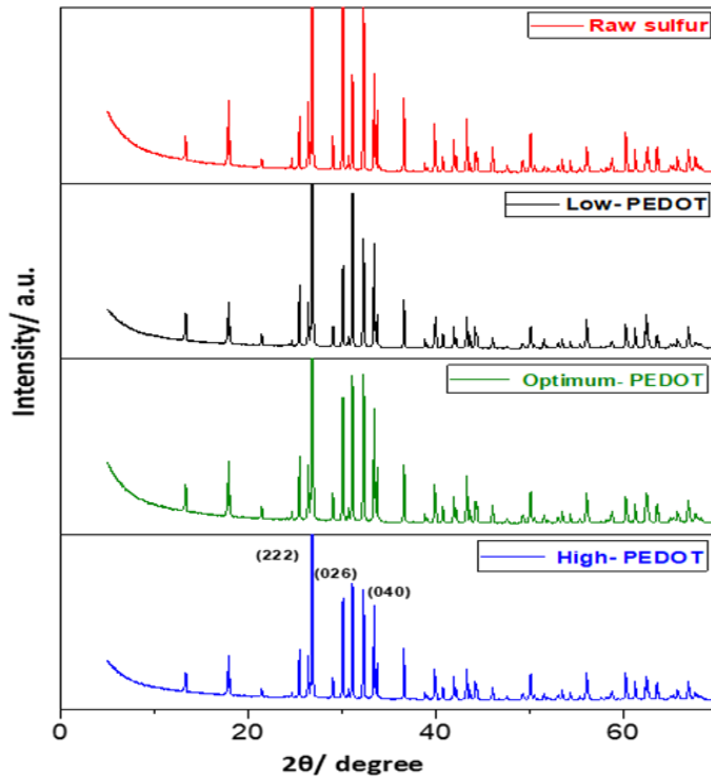


Figure 3: XRD patterns of uncoated sulfur and low-, optimum- and high-PEDOT coated samples.

SEM analysis (Figure 4) was performed to visualize the morphology of the raw and PEDOT-coated sulfur particles. Irrespective of the different amounts of precursor used, all three coated samples show the same particle size and morphology as the raw sulfur and this observation is consistent with the PSD results (Figure S2). In addition, the surface of the particles of the PEDOT-coated sulfur changed in comparison to the commercial raw sulfur. This could be ascribed to the fact that the surface is etched with pitting due to plasma. However, potentially it would be the formation of a PEDOT coating on the surface of the sulfur particles, even if we cannot distinguish the coating morphology between the three-different (low-, optimum- and high-) PEDOT coated sulfur samples, but still, we clearly see the increase in conductivity values (section 3.1). We have tried to perform TEM analysis (Figure S3) in order to obtain more precise information on the PEDOT-coated sulfur powders, especially on the morphology of the PEDOT coating. Unfortunately, sulfur samples were suffering from immediate sublimation under the beam even at low beam intensity. The stabilization of the samples in a matrix was also tried, but the results were not conclusive.

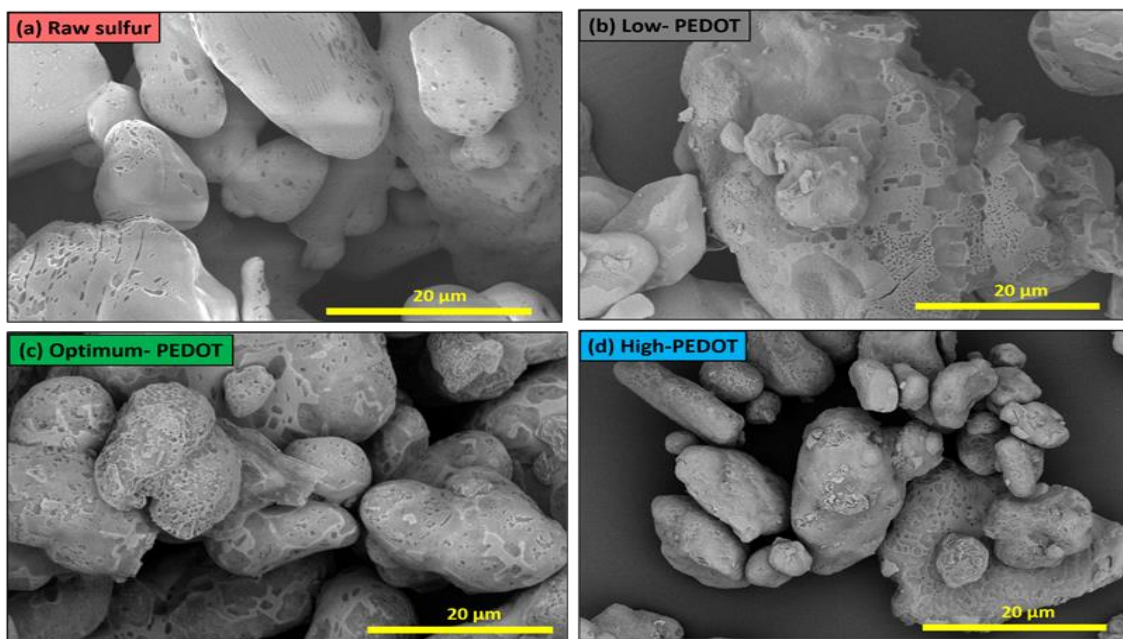


Figure 4: SEM images of a) raw sulfur, b) low-, c) optimum-, d) high-PEDOT coated sulfur respectively.

XPS analysis (Figure 5, S4, Table 2, and S1) was used to characterize the chemical surface composition of the PEDOT-coated sulfur particles. The atomic C/S ratio (Table 2) is 0.6 for the raw and 3.8, 4.3, and 6.1 for the (low-, optimum- and high-) PEDOT sulfur powders, respectively. Similarly, the atomic O/S ratio is 0.09, 1.8, 2.4, and 2.6. These values have to be compared to the ones of the pure PEDOT being C/S = 6 and O/S = 2.⁵³

Table 2: Elemental surface composition (XPS) of coated and uncoated samples.

Sample	Carbon (at. %)	Oxygen (at. %)	Sulfur (at. %)
Raw sulfur	34.3	5.8	59.9
Low- PEDOT	57.7	27.0	15.3
Optimum- PEDOT	55.4	31.7	12.9
High- PEDOT	60.7	26.4	10.0

The evolution of the atomic ratios is in agreement with the deposition of a polymeric coating and the higher amount of EDOT used, the thicker is the polymeric coating. The typical range of the XPS signal depth penetration, i.e. the thickness of surface probed, with standard apparatus is ca. some nm (up to 10 nm). We conclude based on the evolution of the C/S ratio from the different PEDOT coated sulfur powders that the PEDOT-coating thickness is in the nanometer range. The relative high atomic percentages of carbon and oxygen detected on the surface of the raw sulfur (34.3% and 5.8% at., respectively) are attributed to ubiquitous adventitious contamination. This latter is confirmed by the deconvolution of the C1s signal of the XPS spectra (Figure 5), showing a major component due to hydrocarbons (sp^3) the raw sulfur (Figure 5.a) is covered by relatively weak carbon sp^3 signals versus the noise signal. Instead, the C1s signals of the PEDOT-coated sulfur samples (low- 5.b, optimum- 5.b, and high-PEDOT 5.c) are more complex. We conclude from the deconvolution that the polymeric coating (Figure 2 and Table S1) is mostly composed of

sp^2 carbons, which is in agreement with a conductive PEDOT polymer, i.e. π -conjugated polymer, on the surface of the sulfur particles. However, a precise quantification between the sp^2 and sp^3 carbon is challenging due to the small difference between the two signals (< 1 eV).^{51,53,59}

In Figure 5 (a-d) and table S1, the C1s of all three-coated sulfur powders show the main peak at 284.6 eV, which is attributed to the C=C (sp^2 carbon) in the aromatic rings. The higher binding energy peaks at 285.2, 286.7, and 289.0 eV can be attributed to the carbon species of C-C, C-O, or C-S and C=O groups, respectively.

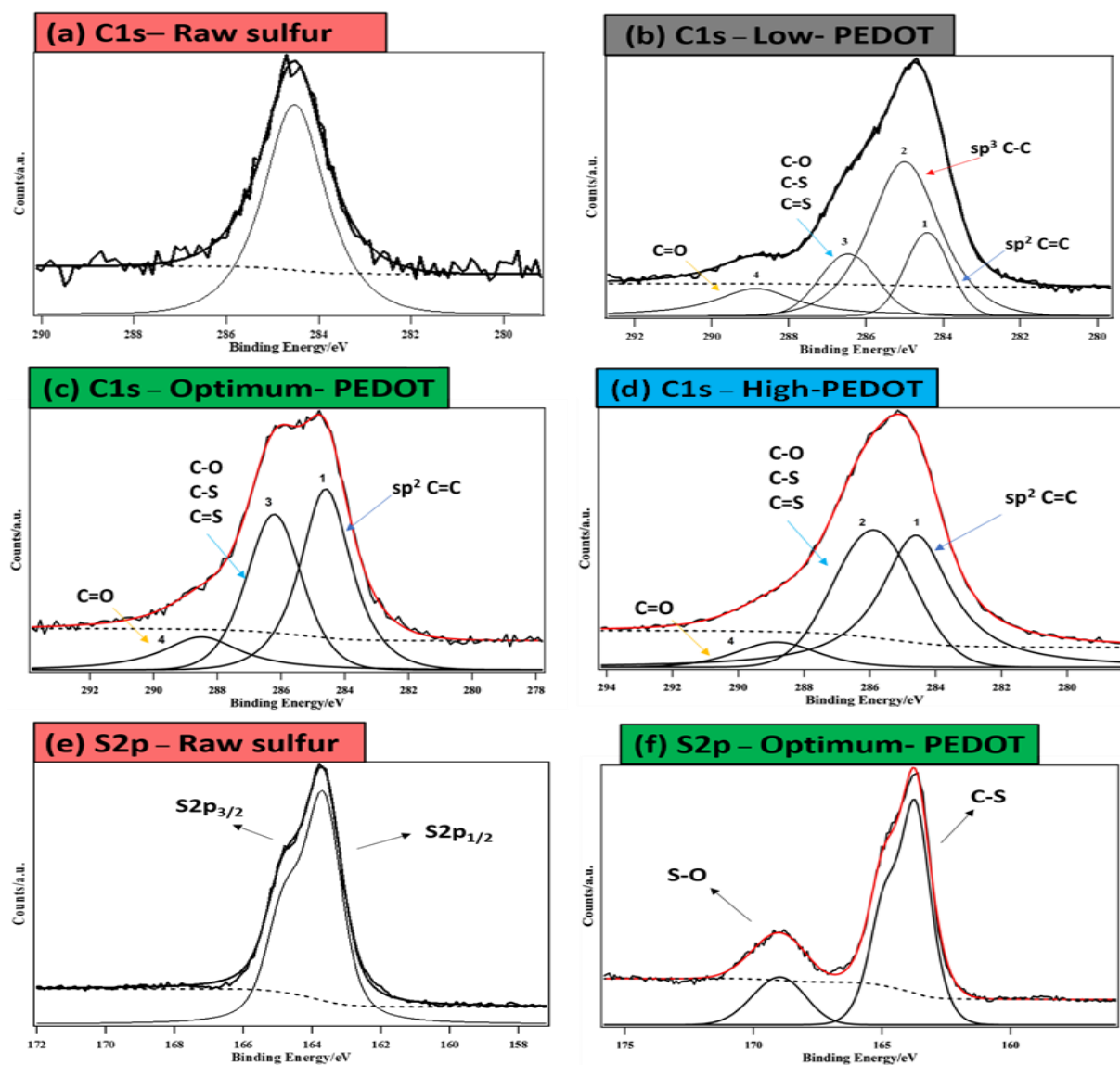


Figure 5: XPS C1s spectra of a) raw sulfur, b) low-, c) optimum-, d) high-PEDOT, and S2p spectra of e) raw sulfur, f) optimum- PEDOT coated sulfur.

No hydrocarbon carbon groups (C–O, C–S, C=S, and C=O) are attributed to the presence of PEDOT coating and accordingly they were not detected on the surface of raw sulfur.⁵¹ The C=O signal is present for all coated samples while at first glance it should not be present for a standard PEDOT-coating. Abessolo et al.⁵³ reported that the DBD-plasma process initiates the EDOT polymerization, but unfortunately other undesired reactions also occur, especially the degradation of the ether ring of the EDOT, leading to the possible formation of C=O groups. In the case of optimum-PEDOT coated sulfur, we observed relatively high intensities of (C=C) functional groups, which relates to high conductivity values (Figure 2) and less capacity fading during electrochemical tests (Figures 8-10 and related discussion in section 3.2). In comparison, the relative intensity of C=C functional groups in the low PEDOT coated sample is weaker than other coated samples, implying a very thin or very limited coverage of conductive polymer on sulfur (in agreement with Raman spectroscopy analysis, Figure 6). In the case of the high-PEDOT coated sample, we also observed the increase in relative intensities of C=O functional groups most probably due to oxidation of the EDOT and PEDOT exposed to the DBD-plasma.

Figure 5 (e-f) displays the S2p spectrum for the raw and optimum PEDOT coated sulfur. The peaks at 165.2 and 164.0 eV can be assigned to the S2p_{3/2} and S2p_{1/2} spin-orbit levels of raw sulfur respectively. In comparison, both pristine sulfur (figure 5-e) and optimum-PEDOT coated sulfur (Figure 5-f) spectra do not allow to confirm if the C-S bonds were actually formed upon the plasma treatment, while oxidized sulfur atoms are clearly present in the latter case, as outlined by the component at higher BE. Consequently, we consider that very low amount (or absence) of C-S bonding between the PEDOT coating and the sulfur particles is formed with the DBD-plasma treatment, while sulfur species on the particle surface are significantly oxidized (i.e. S-O species). We suppose the oxidized sulfur atoms to be the one present on the surface of the S₈ sulfur particles,

taking into account that the sulfur atoms from the PEDOT polymer are stabilized within aromatic rings.

Raman spectroscopy (Figure 6) combined with careful calculations of vibrational spectra is known to provide valuable information for electronic structure. The Raman spectrum of raw sulfur (figure S5) shows three sharp peaks centered at 154, 221, and 475 cm^{-1} respectively, corresponding to characteristic signals of S_8 species.⁵¹ In addition, a clear surface coating effect is observed for all three (low-, optimum- and high-) coated samples, where all coated samples show similar peaks but with lowering peak intensity depending on the amount of precursor used (macroscopic effect), respectively. In Figures 6 (a-d), for a clear understanding of the PEDOT electronic structure, we investigated the region between 1200 and 1700 cm^{-1} where both C=C and C-C stretching vibrations are active.^{60,61,62,63}

For the low- PEDOT coated sample, we did not observe any peak, because of the very thin coating. However, for optimum and high- PEDOT coated samples we observed characteristic peaks that confirm the presence of PEDOT polymer on the sulfur particles. The absorption bands at 1520, 1440, 1370, 1220, and 1140 cm^{-1} are assigned to asymmetric C=C stretching, symmetric C=C stretching, $\text{C}_\beta\text{-C}_\beta$ stretching, $\text{C}_\alpha\text{-C}_\alpha$ inter-ring stretching or CH_2 twisting, and C-O-C deformation, respectively. One additional peak at 1470 cm^{-1} is observed which is attributed to the degradation of the aliphatic chain of the PEDOT polymer (formed by O- CH_2 bond cleavage due to plasma treatment, resulting in $\text{CH}_3\text{CH}_2\text{O-}$ groups) on the surface of the sulfur particles. However, the characteristic absorption band at 1440 cm^{-1} due to symmetric C=C stretching is an indication of good structure retention and high level of conjugation in the structure of PEDOT polymer.^{53,63,64,65} It is reported in the literature^{66,67,68} that, if the peak corresponding to the stretching vibration of C=C becomes narrow, it favours the formation of extended-coil polymeric chains of the quinoid

structure instead of benzoic structure, which increases the π - π stacking in the polymer structure. In comparison with high-PEDOT coated sulfur powder, we clearly observed that in optimum PEDOT coated sulfur powder, the band at 1440 cm^{-1} becomes narrow which indicates the fact that optimum-PEDOT has a longer degree of polymer conjugate length resulting in a higher conductivity value and better electrochemical performance. However, high PEDOT coated sulfur powder potentially shows a wider band which indicates a lower degree of polymer conjugate length. In addition, we have seen an additional peak around 1220 and 1140 cm^{-1} corresponds to CH_2 twisting and C-O-C deformation respectively. This may also be the reason for more degradation of PEDOT during the plasma process, which then further reflects high C=O functional group values and low conductivity as mentioned previously while discussing the XPS results.^{61,62,63}

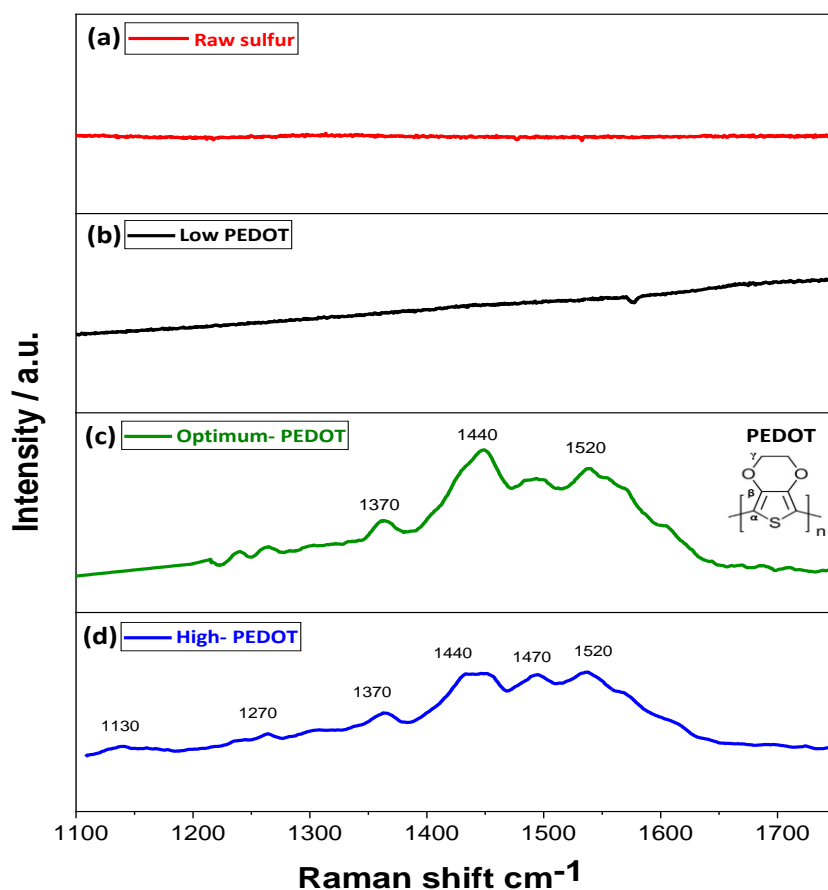


Figure 6: Raman spectra of uncoated and (low-, optimum- and high-) PEDOT-coated sulfur for certain shift region.

In Figure 7, the solid-state ^{13}C -NMR spectrum of the optimum-PEDOT coated sulfur powder confirms the presence of PEDOT in the sample. The signals of PEDOT polymer can be observed in the spectrum at chemical shift positions (in ppm) as expected from literature.⁶⁹ The peak at around 113 ppm can be attributed to the sp^2 carbons next to the sulfur (S), second at around 142 ppm to the sp^2 carbons next to the oxygen (O), and a third around 66 ppm to the sp^3 carbons of the cyclic ethylenedioxy part. However, an aliphatic carbon signal around 30 ppm might be formed by O-CH₂ bond cleavage due to plasma treatment, resulting in CH₃CH₂O- groups of which the CH₃ group can explain the signal. The signal attributed to aromatic C1 carbons is much broader than the reference PEDOT signal found in the literature.⁶⁹ It reveals that, as expected the plasma-polymerized PEDOT coating presents numerous inhomogeneities at the molecular scale compared to PEDOT obtained by standard chemical/electrochemical methods. These inhomogeneities are combination of the presence of α - α , α - β , β - β covalent links while the “pure” PEDOT polymer contains only α - α ones. In addition, many different sub-products and groups are potentially formed from the degradation and opening of the ether ring and can be either remain pendant and incorporated in the main PEDOT chain made with DBD-plasma. Such results also are in agreement with other spectroscopy (XPS, Raman, etc.) data previously reported and explain why PEDOT obtained by DBD-plasma has limited conductivity ($\ll 1$ S/cm level) even if presenting a very homogeneous macroscopic aspect.^{53,65}

To summarize part 3.1, the different characterization techniques are agreeing with each other. A conductive thin polymeric coating was formed using DBD-plasma on the surface of the sulfur particles with a thickness typically of several nanometers. The coating is a PEDOT-type coating but with chemical irregularities (ring opening) caused by the DBD plasma process. The sulfur itself is considered unchanged, only limited aggregation of particles occurred. The highest

electronic conductivity obtained for the optimum-PEDOT coated sulfur is around 10^{-5} S/cm and can be attributed to an optimal surface coverage of the sulfur particles and homogeneities in the polymeric structure of coatings.

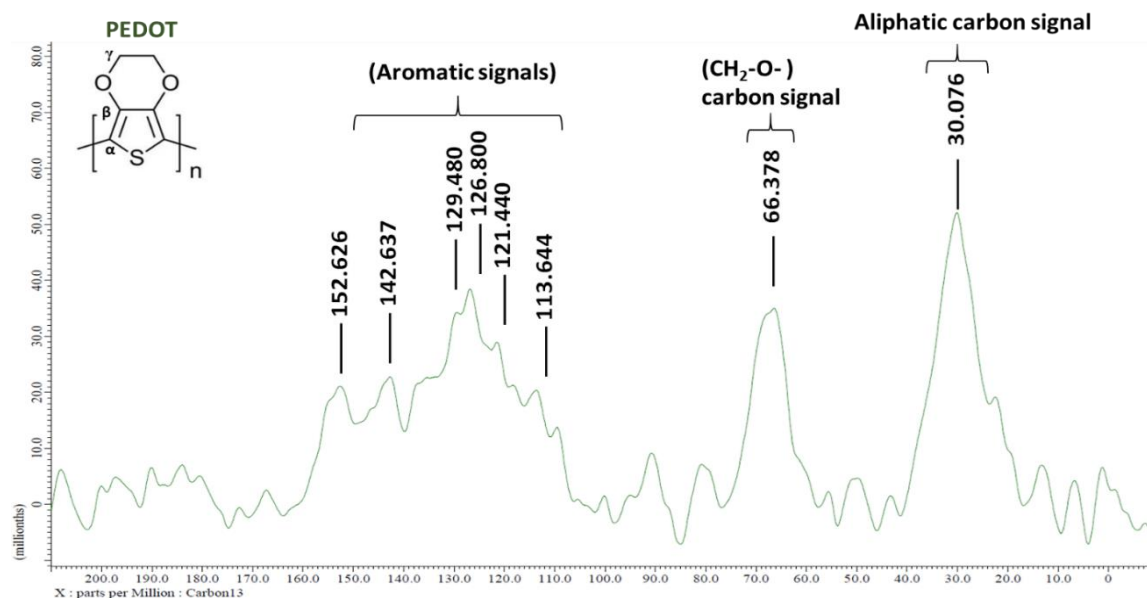


Figure 7: ^{13}C solid-state NMR spectrum of optimum-PEDOT coated sulfur.

3.2: Battery cycling

Charge/discharge performance— Each sample was tested with at least 5 different Li-S cells using an electrode protocol with LiPAA as a binder and (Figure 8 a-d) obtained good repeatability of the electrochemical properties.⁵⁵ Compared to all other samples, the reproducibility clearly improved for Li-S cells containing the optimum PEDOT-coated sulfur powder. A likely explanation is the higher homogeneity within the positive electrodes (both pristine and aged, section 3.4) with improved conductive optimum PEDOT-coated sulfur material, i.e. good electronic percolation. It is supported by the coulombic efficiency vs. cycle (Figure S6), which is obviously the most stable and high ($> 99\%$) for the Li-S cell containing the optimum PEDOT-coated sulfur particles.

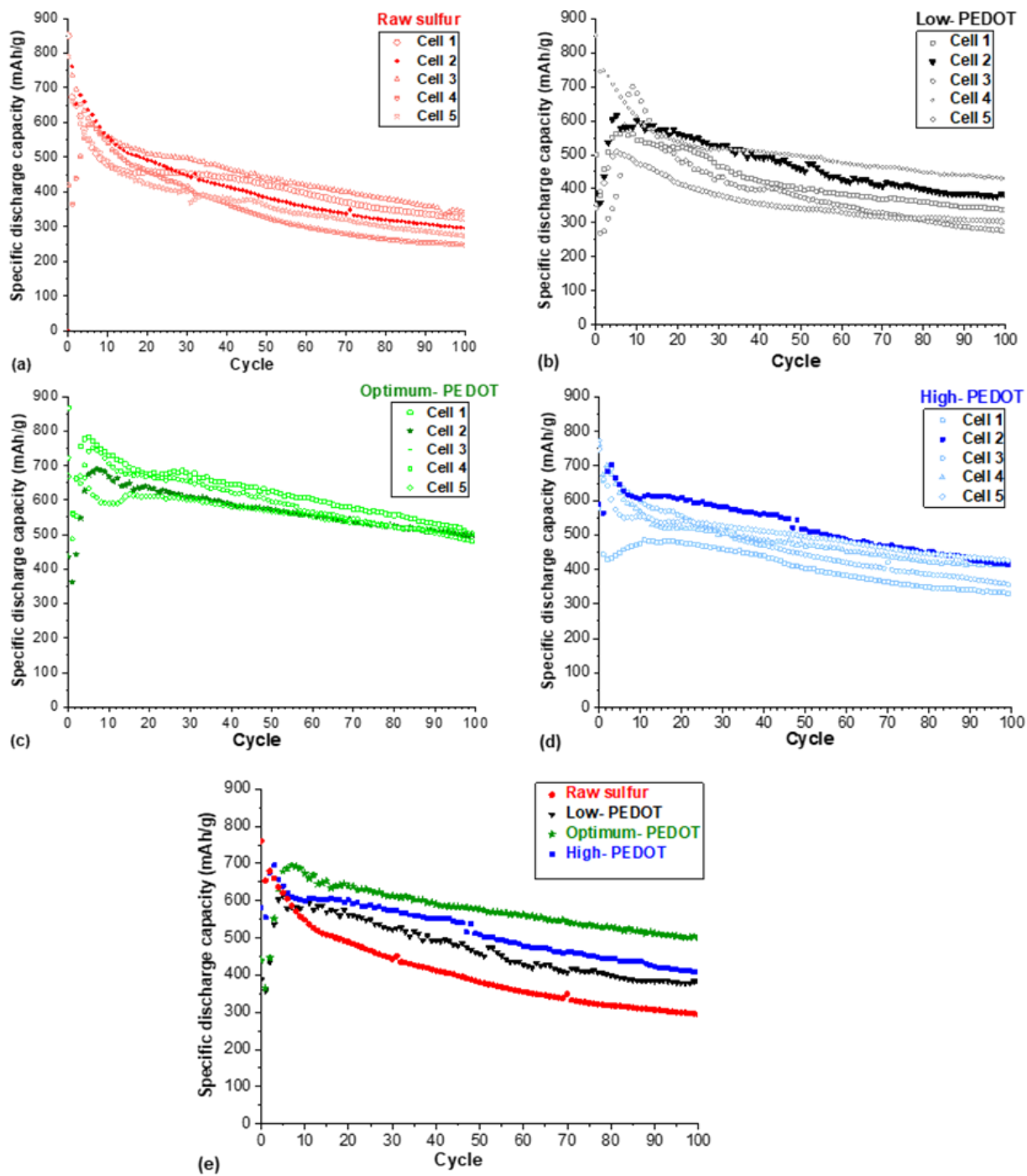


Figure 8: Specific discharge capacity at constant (dis)charge rate ($C/10$) of Li-S electrodes with different sulfur powders present in the electrode (a) raw sulfur, (b) low-, (c) optimum-, (d) high-PEDOT coated sulfur (e) comparison between the cycling ($C/10$) of the most representative Li-S cells using raw sulfur, low-, optimum-, and high-PEDOT coated sulfur respectively.

For the sake of clarity of each sample (Figure 8e), the most representative Li-S cell showing the most regular evolution of the specific capacity versus ageing is presented. The low- and optimum-PEDOT coated sulfur samples present an initial specific capacity almost twice inferior, around 300-400 mAh/g, with respect to the one of the reference raw sulfur, which is around 700-800 mAh/g. Such effect can be attributed to the “activation” of the PEDOT-coating (see later on the galvanostatic profiles discussion). Surprisingly, the high PEDOT-coating does not show such limited initial specific capacity with a value around 600-700 mAh/g or even higher. However, after several cycles, the samples present very similar specific capacity between 600-700 mAh/g. In addition, on prolonged ageing after the 100th cycle, the optimum PEDOT coated sulfur and raw sulfur show discharge specific capacity values of 503 and 297 mAh/g respectively (Table 3). Similarly, the specific capacity fading was calculated to be 18% (1.57 mAh/g/cycle) and 34% (2.20 mAh/g/cycle) between the 30th cycle and 100th cycle. These first results already confirm the effectiveness of the PEDOT-coating by DBD-plasma on sulfur powder to improve the properties of Li-S batteries, especially the mitigation of the capacity fade, and the characterization data (see part 3.1).⁷⁰ However, for the case of low and high PEDOT coated sulfur vs. raw sulfur, the continuity of PEDOT-coating layer is not as clear (as expected from the characterization data discussed in part 3.1). Low- PEDOT coating sample has a too thin coating and poor conductivity (two orders less than the best sample). The high PEDOT-coating sample possesses a thick coating but with many inhomogeneities, at least at the polymeric chain scale (see Figure 6 and related discussion), also leading to limited conductivity.

More importantly, when comparing previously published results using similar polymeric coatings, the Li S cells of this study appear at least to be as good capacity retention if not better, especially taking into account the high sulfur loading of our electrodes.^{25,26,42,44,46,51,71,72,73,74} In addition, the

here applied surface coating protocol (by using DBD-plasma) is straightforward, uses only standard, cheap, abundant, and relatively low toxic chemicals and small quantities (exception of the sulfur itself of course). It does not require high temperature (risk of sulfur fusing), neither high pressure (risk of explosion) nor long time, and neither vacuum drying step (risk of sulfur sublimation) and already kg/day scale production can be reached. We consider that the protocol presented here is of interest for upscaling and compatible with the production of pouch cells at least at laboratory or pilot scales. The latter was recently described by Dörfler et al.⁷⁵ to be essential for testing in order to evaluate relevant scientific progress in the field of Li-S pouch cell technology.

Table 3: Summary of discharge capacity at 30th, and 100th, specific capacity fade, and average coulombic efficiency between the 30th and 100th cycle for the raw sulfur, low-, optimum- and high-PEDOT coated Li-S cells (from Figure 8e and Figure S6).

Sample	30 th Discharge Capacity (mAh/g)	100 th Discharge Capacity (mAh/g)	Capacity Fade % (from 30 th to 100 th Cycle)	Capacity Fade per cycle from 30 th to 100 th Cycle (mAh/g/cycle)	Average coulombic efficiency from 30 th to 100 th Cycle (mAh/g/cycle)
Raw sulfur	451	297	34	2.20	99.00
Low- PEDOT	522	383	27	1.99	98.80
Optimum- PEDOT	613	503	18	1.57	99.40
High- PEDOT	573	407	29	2.37	99.30

The (dis)charge mechanism of the Li-S battery is very complex and sensitive to many parameters including, but not limited to, current density, temperature, type of electrolyte, and polymeric coatings.^{13,76} The initial galvanostatic discharge cycles in Li-S cells with uncoated and coated sulfur show an anomalous profile (Figure 9.a). The discharge capacity is limited for cells showing a continuous potential drop throughout the discharge and the expected voltage plateau at 2.0 V vs. Li⁺/Li is absent. This might be explained by a microstructural rearrangement within the porous electrode due to the volume changes during the (dis)charge step. We did not report such anomalous

first discharge previously with raw sulfur and LiPAA as binder.⁵⁵ However, in the present case, the areal sulfur loading was increased by 12.5% up to 4.5 mg/cm². We have observed more anomalous profile of the first discharges for sulfur electrodes using our protocol and with such high loadings.⁷⁷ The (dis)charge galvanostatic profile of the raw sulfur-based cell (Figure 9.b-c) follows the expected trends reported in the literature^{55,70} for oxidation and reduction of a sulfur electrode in DME/DOL solvent.

At the early stage of the reduction, a potential drop towards a first voltage plateau at ca. 2.3 V vs. Li⁺/Li is observed. It is followed by a second voltage plateau at 2.0 V vs. Li⁺/Li before a fast and final potential drop until the lower voltage limit of 1.5 V vs. Li⁺/Li. The latter plateau corresponds to more than 50 % of the total discharge capacity. The galvanostatic discharge profile corresponds to the reduction of the S₈ to Li₂S, both solids, with the formation of intermediate polysulfides Li_xS_y. The specific capacity remains in any case much lower than the theoretical value of 1675 mAh per gram of sulfur, mainly due to a significant part of the α-S₈ which remains unreacted. The charge profile is characterized by a strong hysteresis and monotonous potential increase to a plateau around 2.4 V vs. Li⁺/Li at which 75% of the total charge capacity is delivered.⁵⁵ However, the (dis)charge capacity is limited for cells with (low-, optimum-, and high-) PEDOT coated sulfur. During the 3rd discharge, all coated samples show a potential drop throughout the discharge and the voltage plateau at 2.0 V vs. Li⁺/Li is very limited. In addition, at the early stage of the first oxidations (Figure 9.a and 9.b), all cells containing a PEDOT-coated sulfur material present a significant overpotential at the early stage of the oxidation when compared to the cell with raw sulfur. Starting the 5th cycle (Figure 9.c), all Li-S cells (with and without coating on the sulfur) show standard (dis)charge profiles. The overpotential at the beginning of the charge is severely reduced with the coated sulfur materials (even not present for the high-PEDOT). More

interestingly, starting the 15th cycle (Figure 9.d), the situation between the cells with raw sulfur and the coated sulfur is reversed, versus the 1st cycle when taking into account the specific capacity and voltage hysteresis respective values. Consequently, we consider the anomalous initial galvanotactic profiles of the Li-S cells containing the coated sulfur materials to be due to supplementary rearrangement mechanisms or activation induced by the presence of the PEDOT coating.

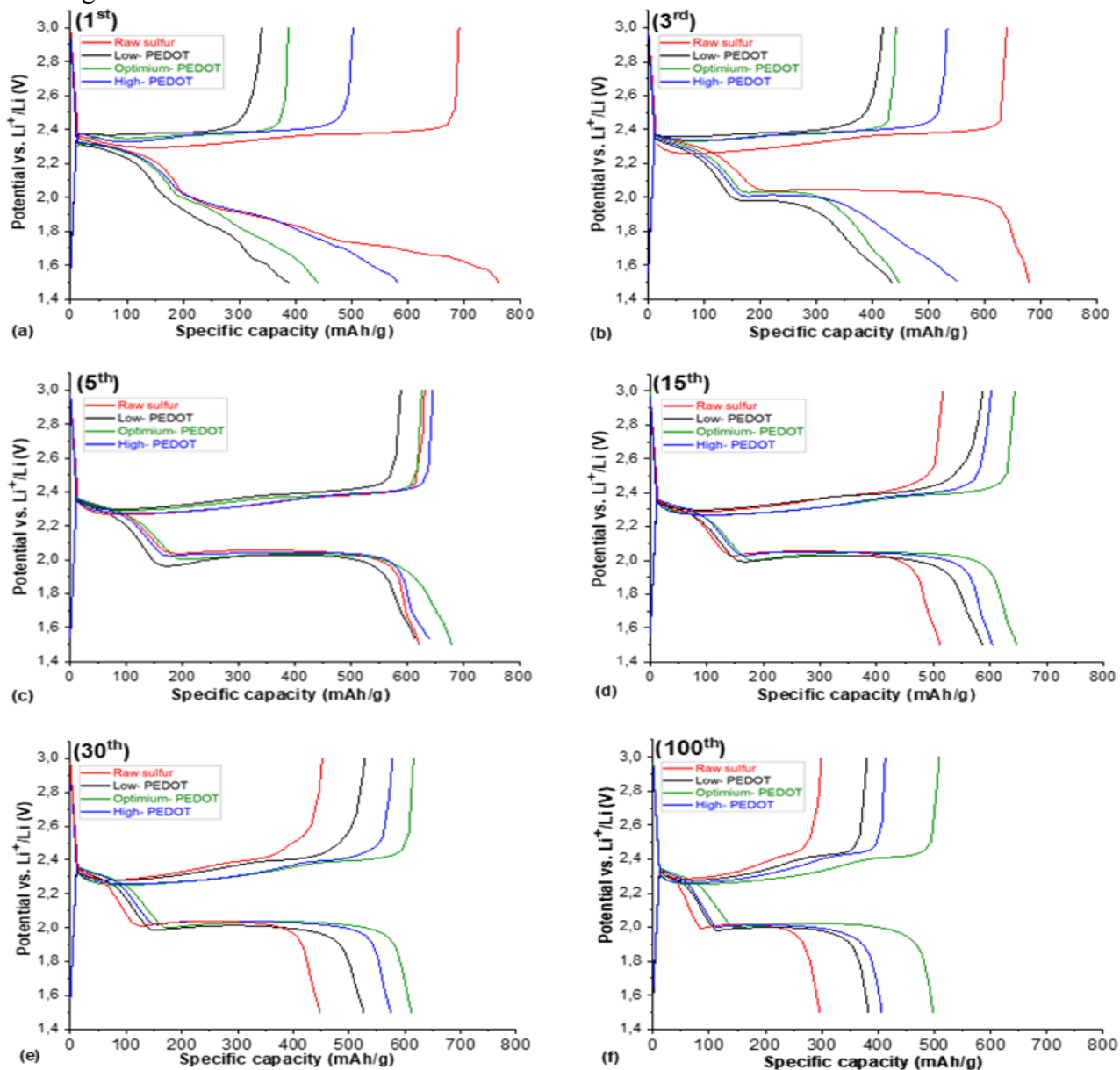


Figure 9: Galvanostatic (dis)charge (C/10) profiles of Li-S cells with raw sulfur, low-, optimum-, high-PEDOT coated sulfur respectively at a) 1st, b) 3rd, c) 5th, d) 15th, e) 30th and f) 100th cycle.

For the medium-term cycling (30th cycles, Figure 9.e), the Li-S cell using optimum-PEDOT has a capacity of ca. 162 mAh/g higher than that of the cells with raw sulfur (see Table 4). The voltage plateau at ca. 2.0 V, labeled as C_L, is shorter while the capacity at the early stage of discharge between 2.0 and 2.4 V vs. Li⁺/Li, referred as C_U, is almost identical for the four samples. We then consider that the presence of the PEDOT-coating is not changing any electrochemical reaction occurring in the Li-S cells but just has an effect on the kinetics (see latter).

Table 4: From Figure 9 values of the upper plateau discharge between 2.1-2.4 V vs. Li⁺/Li, labeled C_U, the lower discharge plateau at ca. 2.0 V vs. Li⁺/Li, labeled C_L. The total discharge specific charge is labeled as C_U + C_L = C_T for the 30th and 100th cycle.

Sample	30 th Cycle			100 th Cycle						
	C _U	C _L	C _T	C _U /C _T	C _L /C _T	C _U	C _L	C _T	C _U /C _T	C _L /C _T
	(mAh/g)			(%)		(mAh/g)			(%)	
Raw sulfur	128	323	451	28	72	81	216	297	27	73
Low- PEDOT	150	372	522	29	71	109	274	383	28	72
Optimum- PEDOT	181	432	613	30	70	156	347	503	31	69
High- PEDOT	146	427	573	25	75	110	297	407	27	73

On long-term cycling (at 100th cycle, Figure 9.e), the capacity fade is less pronounced for the Li-S cells with (low-, optimum- and high-) PEDOT coated samples compared to the cells made with raw sulfur. The shape of the (dis)charge profile of the Li-S cell with raw and (low-, optimum- and high-) PEDOT coated sulfur samples remains mostly unchanged even after 100 cycles at C/10 in contrast to the cells with raw sulfur. A more detailed analysis of the capacity data between the 30th and 100th cycle shows that the C_U in discharge decreases by 37 %, 27 %, 14 %, 24 %, and for the cells with raw sulfur, low-, optimum- and high- PEDOT coated samples compared respectively.

The capacity fade for the C_L part of the discharge is 33 %, 26 %, 19 %, and 30% respectively. Globally, the cathodic capacity fade during ageing is equally represented in C_L and C_T parts of the reduction occurring in the positive electrodes. In addition, the potential hysteresis for Li-S cells made with raw and (low-, optimum- and high-) PEDOT coated sulfur-based positive electrodes increases for all cells during ageing (Figure S7). However, the hysteresis increase is much limited in the case of the optimum-PEDOT coated sulfur ~ 8 mV, while it is superior at 55, 40, 30 mV for raw, low- and high- PEDOT coated sulfur samples respectively.

The optimum-coated PEDOT sulfur has already clearly shown a superior behavior as active material in the sulfur-based electrode of the Li-S cells. So, the next steps of the discussion focus on comparing only the raw and optimum-PEDOT coated sulfur materials. The influence of the current density during galvanostatic cycling is presented in Figures 10 and S8. As expected, increasing the current density leads to decrease in the specific capacity of the raw and optimum-PEDOT coated sulfur materials. The rate capability of the Li-S cells (Figure S8.f) using the optimum-PEDOT sulfur is larger than the ones using raw sulfur. The cells using raw sulfur at $C/5$ and $C/10$, show globally a superior and significant increase of the hysteresis width between discharge and charge in comparison to the cells using optimum-PEDOT as a polymeric coating (Figure S8.a-e).

The different electronic properties (for conductivity at the surface of the sulfur powder and electron transport R_{ct} in the electrode see Figures 2 and 12 and related discussion, respectively) between the raw and optimum-PEDOT coated sulfur seem to be the main factor to be taken into account to explain these phenomena. Both Li-S cells containing either the uncoated and coated sulfur materials show almost zero capacity when reaching 1C rate. However, the capacity is regained for all cells when returning back to the $C/10$ rate. **At the first look, it can be considered that the**

performance of our Li-S cells is limited compared to the literature for both the specific capacity and the rate of (dis)charge, especially at 1C. As mentioned in our last publication⁵⁵ this might be explained by the fact that we are using sulfur particles (commercially available) with large granulometry ($d_{50} > 10 \mu\text{m}$ diameter and $d_{99} > 100 \mu\text{m}$ diameter). Easy and safe production of fine sulfur powder is a challenge.⁷⁸ We are currently working on the optimization of the granulometry of the sulfur particles and electrode engineering to obtain better electrochemical performances of our Li-S cells. Besides, our sulfur electrodes contain a limited amount of additive carbon (24% in weight) and the high loading of sulfur electrodes ($\sim 4.5 \text{ mg/cm}^2$) is also to be taken into account. These parameters are often neglected in most publications and are necessary to be considered to make the Li-S batteries fit for practical application in the future.¹³ Besides, in the present report our goal is to validate the concept of powder coating with DBD-plasma technologies associated with all its advantages (one step, no solvent, ambient pressure, low energy consumption), i.e. up scalable and sustainable. Our present production of PEDOT-coated sulfur powder can reach the kg/day scale and appears compatible with up-scaling. Moreover, in near future, we are planning to investigate our material with pouch cell configuration. This corresponds to a capacity increase ($> 1 \text{ Ah}$) to at least 100 times versus coin-cells, which is a critical point to get the practical application.

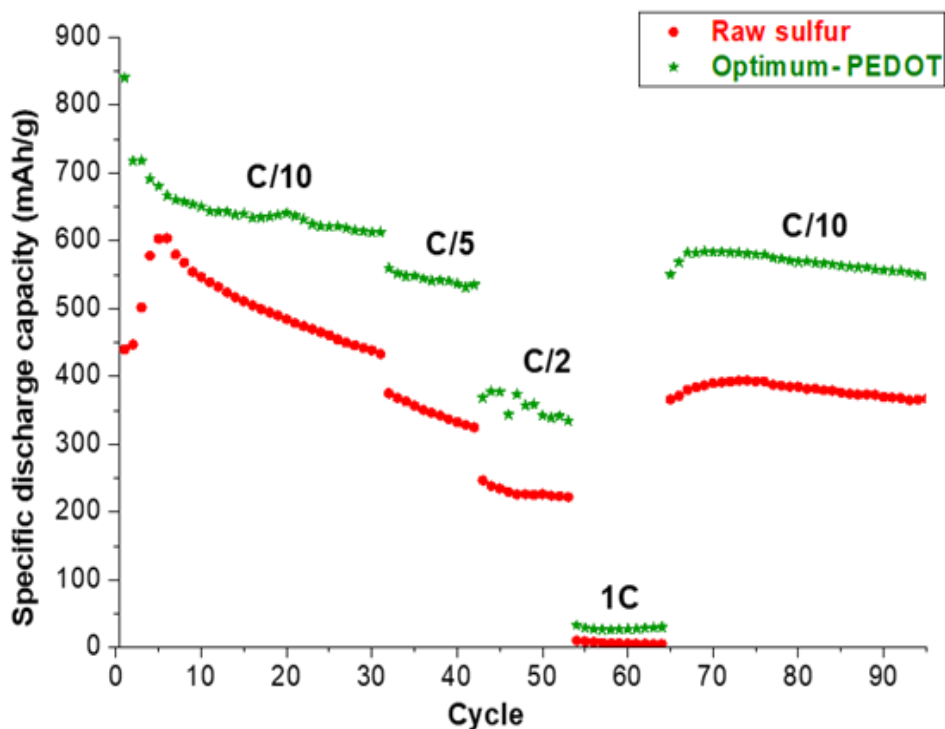


Figure 10: Discharge capacity at different discharge/charge rates for Li-S cells using raw sulfur (red) and optimum-PEDOT coated sulfur (green) in the positive electrode.

To evaluate more precisely the influence of the raw and optimum-PEDOT coated samples on the kinetics of the electrochemical reactions occurring during the cycling in the Li-S cells, cyclic voltammetry (CV) at different scan rates were measured (Figure 11, Figures S9 and S10, and Table S2). At low scan rate of 0.1 mV/s, the shape of the CV using electrodes containing either raw or optimum-PEDOT coated sulfur are globally similar with one anodic peak and two reduction peaks (as expected). However, we can notice that all the peaks, anodic and cathodic, are clearly sharper and the potential hysteresis is significantly limited in the case of the latter (Figure S10.a). It already confirms that the electrode containing the optimum PEDOT-coated sulfur present facilitated electrochemical kinetics in comparison to the electrode with raw sulfur. When increasing the scan rate from 0.1 to 2 mV/s, changes in the shape of the cyclic voltammetry and the shift of the peaks (higher hysteresis) occur in both cases, but it is clearly more pronounced for the raw sulfur electrode, thus confirming our first observation at low scan rate. Consequently, it is clear that the

kinetics of the electrochemical reactions of the sulfur species in the Li-S cells can be classified as optimum-PEDOT is highly superior to raw sulfur-based Li-S cell, which is attributed to the presence of a conductive coating on the sulfur particle, similarly to Raulo et al.⁷¹ In addition, anodic linear sweep voltammetry (LSV) from 1.5 to 5.0 V vs. Li⁺/Li with bare Al-foils and Al-foils with coated PEDOT polymeric film (Figure S11) showed that the PEDOT is not initiating any further reaction and is stable in the potential range used to test our Li-S cells.

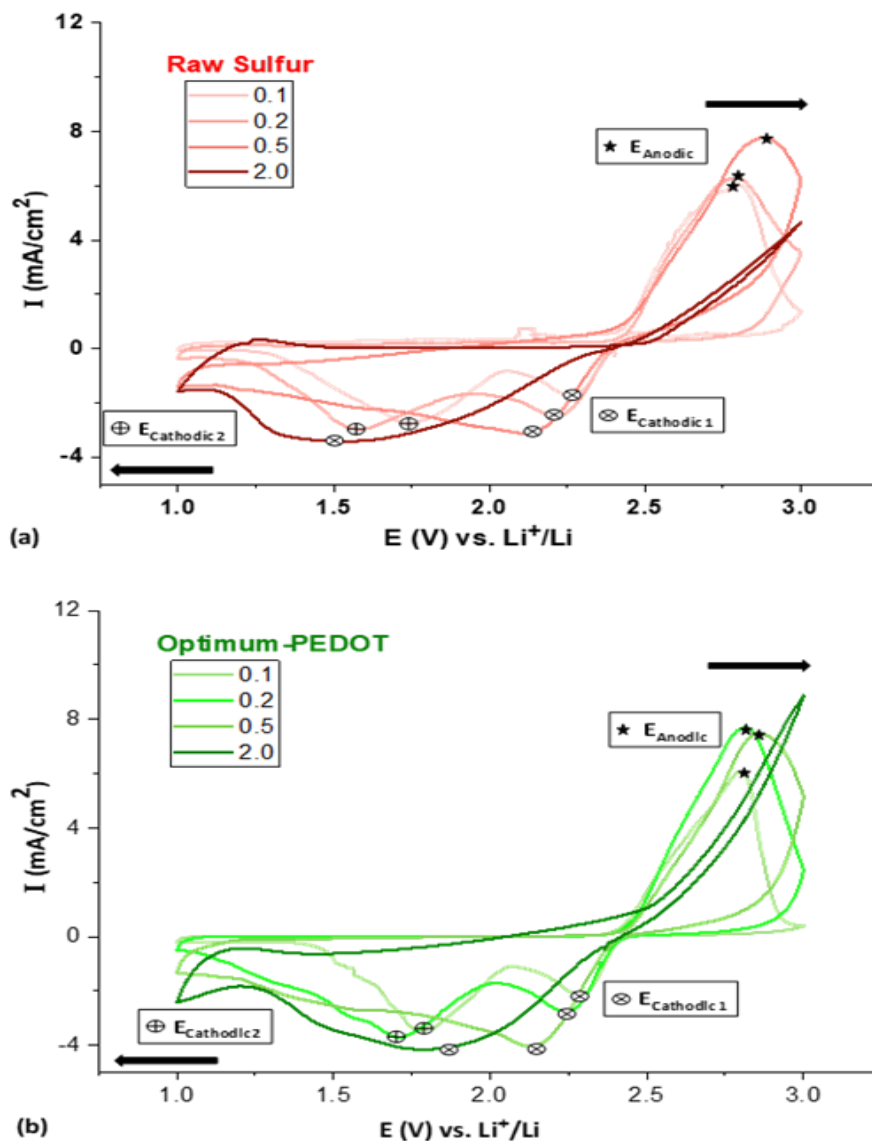


Figure 11: Cyclic voltammetry of (a) raw sulfur-based, (b) optimum PEDOT coated sulfur-based electrodes at 0.1, 0.2, 0.5 and 2 mV/s. The symbols on cyclic voltammetry are the values of the cathodic and anodic peaks reported in Table S2.

3.3: Electrochemical Impedance Spectroscopy (EIS)

The electrochemical impedance spectroscopy test (10 mHz to 300 kHz) is presented for Li-S cells (Figure 12) made with raw and optimum-PEDOT coated sulfur-based electrodes before the first (dis)charge and after 70 galvanostatic cycles. Pristine electrodes at OCV state (Figure 12.a) show a standard shape with a semi-circle at higher frequencies followed by an inclined line at lower frequencies. The optimum-PEDOT coated sulfur material shows a charge transfer resistance, R_{ct} (semi-circle diameter) value at $\sim 15 \Omega$, at least three times smaller than the electrode containing the raw sulfur ($\sim 50 \Omega$). Similarly, the slope of the following inclined line (known as Warburg element) is significantly steeper for the former than the latter with values of 0.84 and 0.40, respectively. It appears that both the electron transfer and the Li-ion transport in the sulfur electrode are facilitated with the presence of the optimum PEDOT-coating sulfur powder in the pristine electrode. This is in agreement with the literature^{79,80,81} and previous parts of the discussion 3.1 and 3.2.

The shape of the Nyquist plots of aged electrodes after 70 cycles (Figure 12.b) evolved radically due to important changes occurring in the electrodes with the successive dissolution-precipitation mechanisms of the sulfur species. Both raw and optimum-PEDOT coated electrodes exhibit decreased R_{ct} values (first semi-circle at higher frequencies, diameter shrinks) with 9 and 13 Ω , respectively, in comparison to the pristine electrodes. (Figure 12.a). In the aged electrodes, we consider that the liquid/solid interface is improved in comparison to the pristine ones. We also notice that the aged Li-S cells show an electrolyte resistance of 10 and 5 Ω for the Li-S cells containing the optimum-PEDOT coated sulfur and the raw sulfur, respectively. It can be due to different effects as the aforementioned electrolyte degradation (but in this case minimal to counter the other advantages of the presence of the PEDOT-coating), possible dissolution of EDOT and/or

PEDOT-oligomers not covalently attached to the coating, or more polysulfide remaining in the electrolyte. The second semi-circle at medium-frequencies is usually attributed to the formation of solid lithium-polysulfide (Li_2S_2 and Li_2S). It is again significantly smaller for the optimum PEDOT-coated sulfur than the raw sulfur material with values at 5 and 26 Ω , respectively (note these values are approximate and have to be considered as semi-quantitative).^{26,42,71}

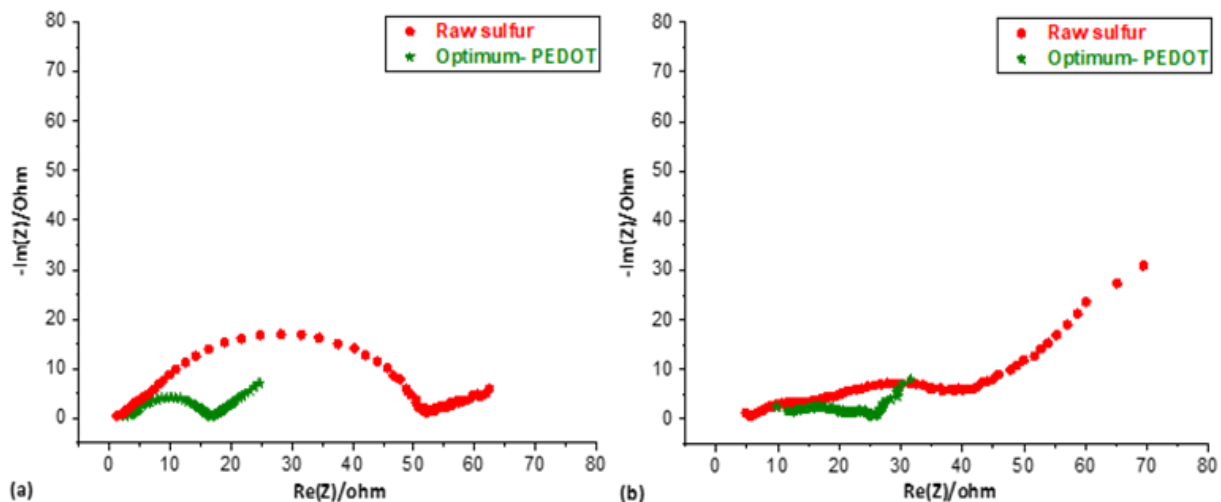


Figure 12: Nyquist plots for Li-S cells at OCV using raw (red) and optimum-PEDOT coated (green) sulfur-based (a) pristine electrodes and (b) the same electrodes after 70 galvanostatic cycles at C/10.

3.4: Post mortem analyses (SEM)

One can object that the advantageous electrochemical properties of sulfur electrodes containing the optimum-PEDOT coated sulfur may not be only due to the presence of the conductive polymeric layer on the sulfur particles, but other phenomena must be considered as possible macroscopic effects (electrode morphology and its evolution) when different sulfur powders are used. Post mortem SEM and BET analyses were therefore performed.

Positive electrodes with raw and optimum PEDOT-coated sulfur show very similar (identical) morphologies at pristine state (Figure 13.a to 13.d). After 2 cycles and at low magnification, the

electrode with raw sulfur (Figure 13.e) seems to be wider fractured than the one containing the coated sulfur (Figure 13.f) but this observation is not valid at higher magnification (Figures 13.g and 13.h). In addition, the inverse can be seen after 70 cycles (Figure 13.i and 13.j). A similar conclusion arises for the unwashed positive electrodes (Figure S12). Similarly, post-mortem analyses (SEM and EDX) on the non-washed negative electrode (Li-metal) do not allow us to distinguish between the cells using raw sulfur and the ones using the coated PEDOT (Figure S13 and S14). This may seem counter-intuitive as the presence of PEDOT in the positive electrode is expected to act as a polysulfide trap, limiting polysulfide shuttle phenomenon. We explain this by the fact that the PEDOT-coating is probably not a defect-free membrane. In addition, the total charge throughput, i.e. the amount of polysulfide formed at all was clearly superior for the cell with PEDOT-coated sulfur than the one with the raw sulfur.

In order to have a better understanding of the structural integrity of both coated and uncoated sulfur electrodes, we have measured the N₂-sorption and BET analyzes of the pristine and cycled cells (electrodes) after 70 cycles (Figure 14 and Table S3). The N₂ adsorption profiles are similar for all the types of electrodes (both pristine and cycled) independent of the polymeric coating present, all with the same order of surface area and porous size. Due to the limited amount of material characterized for each measurement, the data obtained from the N₂-sorption must be considered as semi-quantitative at the best. Thus, the difference between the electrodes (raw and coated sulfur, pristine and cycled electrodes) is not significant. Consequently, the microstructure is said to be similar for all electrodes, as already concluded from the SEM results (Figure 13.a-d, i-l). The superior electrochemical properties (parts 3.2 and 3.3) of the Li-S cells containing the PEDOT-coated sulfur is solely attributed to the presence of polymeric conductive coating on the surface of the sulfur particles.

Note that the post-mortem analyses confirm the high stability of the structure of the sulfur electrodes using our protocol even after 70 cycles at full charge/discharge with a C-rate of C/10, even, if it was not the primary goal of this study.

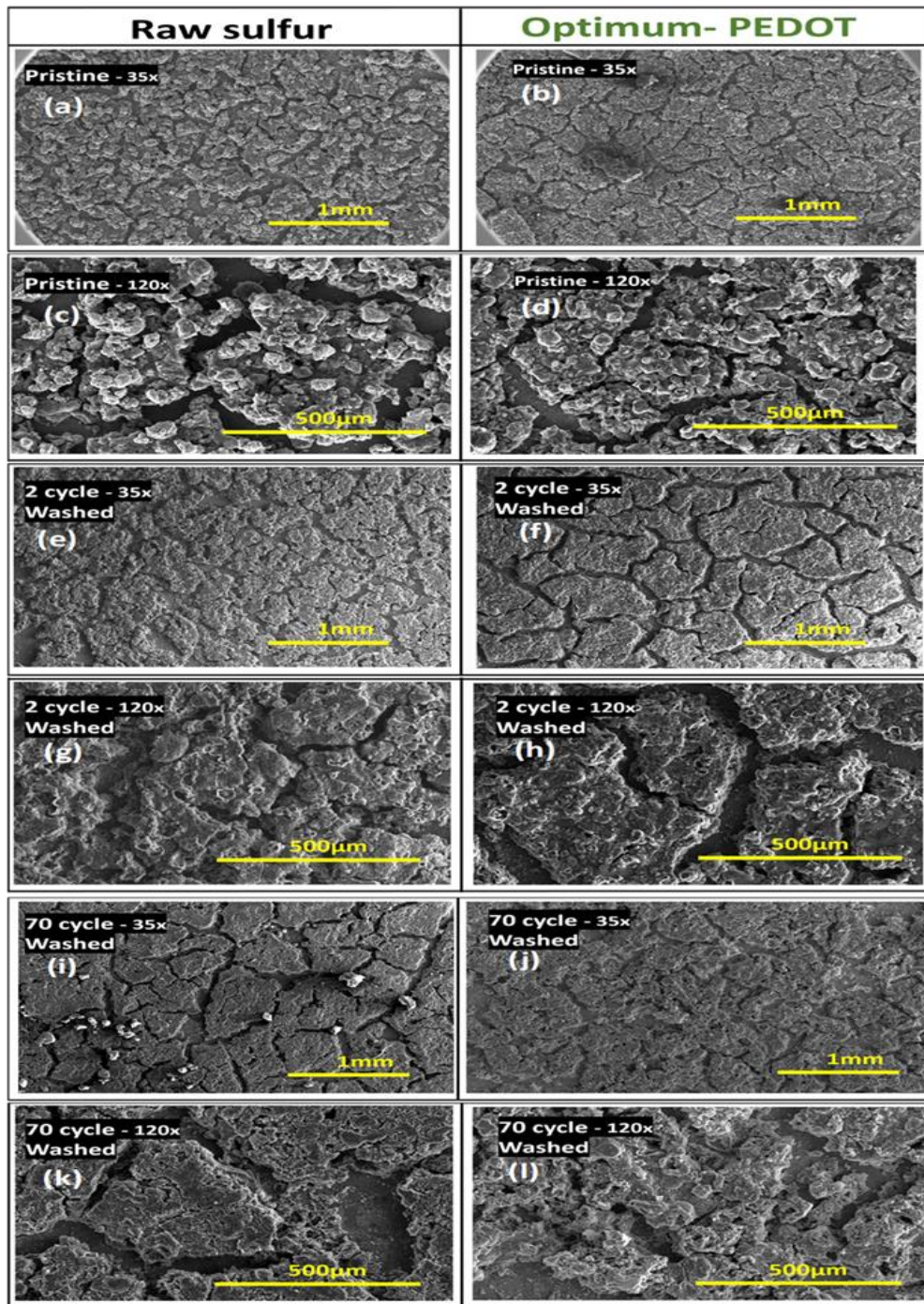


Figure 13: SEM images of sulfur electrodes with raw and optimum- PEDOT coated samples at different magnifications, and different state of cycling: pristine, after the 2nd and the 70th cycle (C/10). The electrodes were recovered and washed after a full discharge followed by 1h rest at OCV.

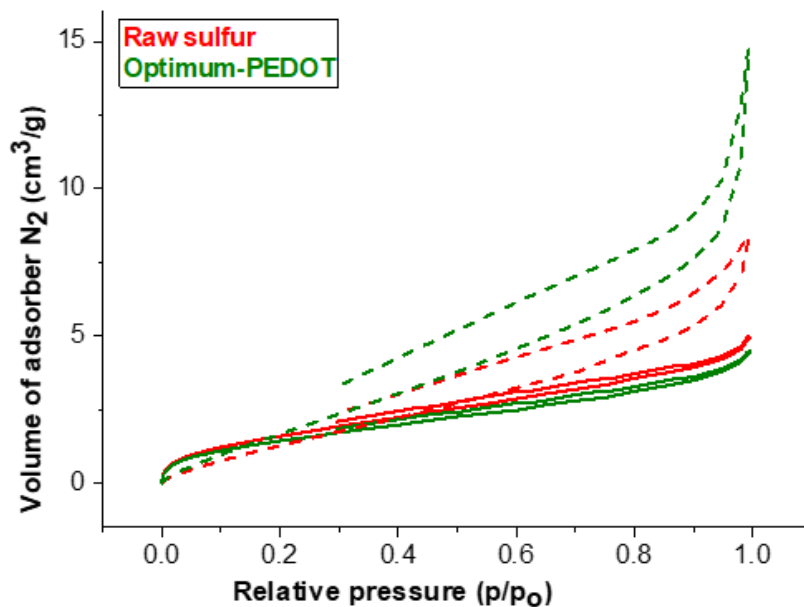


Figure 14: N₂ adsorption isotherms of the pristine (solid lines) and cycled (70th cycle, dashed lines) sulfur electrodes using raw sulfur (red) and optimum-PEDOT coated sulfur (green) in Li-S cells. Note that the adsorbed volumes were corrected.

4.0 Conclusions

In this work, we have successfully applied conductive PEDOT-coating on the surface of sulfur particles using DBD-plasma technology. The coating protocol using atmospheric conditions (low temperature and ambient pressure) is easy, one-step, fast, dry (no toxic solvent and no solvent removal step), and it is compatible with upscaling, presently kg/day at laboratory scale. Our coating process entails low cost, safe, low energy consumption and low risk, which makes it compatible with the urgent need for more sustainable technologies. Moreover, the DBD-plasma treatment is compatible with the manipulation of very fragile materials such as elemental sulfur (easily sublimate & oxidize, low melting point, and burnable). The DBD-plasma treatment does not lead to any change in the bulk properties of the sulfur particles (S₈ crystal structure and particle morphology). The surface electronic conductivity is increased up to 10⁻⁵ S/cm in the case of the optimum PEDOT coated sulfur powder and remains stable for more than 6 months. The presence of the PEDOT coating was confirmed by XPS, Raman, and NMR spectroscopy. Raman

spectroscopy proves that at the polymeric chain scale the PEDOT-coating itself is more regular for the optimum PEDOT-coated samples than the high PEDOT-coated sulfur samples, and hence justifies why their conductivity is 10^{-5} and 10^{-6} S/cm respectively. NMR spectroscopy confirms that the plasma-polymerized PEDOT coating has a different and less regular chemical structure compared to conventional PEDOT coating.

The electrochemical tests (with high sulfur loading ~ 4.5 mg/cm²) confirm the superior behavior of the optimal PEDOT-coated sulfur powder when used in the positive electrode for Li-S cells, in terms of specific capacity, coulombic efficiency, aging, and these results are highly reproducible. More intensive investigations confirm that the optimum PEDOT-coated sulfur leads to higher charge-rate capability, faster electrochemical kinetics, and lower internal resistance. All these results are explained by the presence of a conductive polymeric coating on the surface of the sulfur particles. In addition, post-mortem SEM and BET analyses for both uncoated and coated sulfur electrodes allow us to exclude any significant effect at the electrode scale.

Further developments are ongoing, involving optimization of the granulometry of the sulfur powder by sulfur milling (smaller and sharper PSD) before coating. Also, to improve the conductivity and mechanical strength of the coating, different optimization strategies such as chemical doping (acid, MgO₂) or increasing the molecular cross-linking of the PEDOT (plasma reactor parameters, doping with thiophene) are foreseen.

Realizing Li-S cells, suitable for a commercial application is still an open challenge both for the manufacturers and for the scientific community. This work presents very promising results, touching different fundamental aspects of these complex battery systems and depict possible ways for further investigation works. Last but not least, the possibility to perform powder coatings in

dry and low temperature conditions opens possibilities for straightforward surface functionalization of standard lithiated metal oxides (LiCoO₂, NMC) that suffer from manipulation in water or cannot be heat-treated (at high temperature) to obtain standard conductive carbon coating.

ASSOCIATED CONTENT

Supporting Information

Additional tables and figures including complementary information on the coating synthesis and electrochemical characterization of both uncoated and coated sulfur powders.

The following files are available free of charge.

AUTHOR INFORMATION

Corresponding Author

An Hardy, * (Email: an.hardy@uhasselt.be)

Sébastien Sallard* (Email: sebastien.sallard@vito.be)

Author Contributions

Ahmed Shafique: Investigation, Visualization, Validation, Writing & editing- original draft.

Vijay Shankar Rangasamy: review & editing, Validation.

Annick Vanhulsel: review & editing, Validation.

Mohammadhosein Safari: review & editing, Validation.

Silvia Gross: review & editing, Validation.

Peter Adriaensens: review & editing, Validation

Marlies K. Van Bael: review & editing, Validation.

An Hardy: Supervision, review & editing, Validation.

Sébastien Sallard: Conceptualization, Supervision, Writing - review & editing, Validation

Funding Sources

The authors declare that they have no known competing financial interests or personal relationships that could have appeared to influence the work reported in this paper.

ACKNOWLEDGMENT

The authors are grateful to Imerys Graphite & Carbon for providing the C-nergy Super-C65. The authors are thankful to Fulya Ulu, Andreas Paulus, Gunter Reekmans, Bert Verheyde, Anne-Marie De Wilde, Danny Havermans, Erwin Van Hoof, Myrjam Mertens, and Raymond Kemps for their help and support in the laboratory, the characterization of the samples, and the analysis of the data. Dr. Stefano Diodati is gratefully acknowledged for support in the elaboration of XPS data. NMR work is supported by Hasselt University and the Research Foundation Flanders (FWO Vlaanderen; Hercules project AUHL/15/2 - GOH3816N).

REFERENCES

- (1) Dudley, B. *BP Statistical Review of World Energy 2014*; 2014.
- (2) Julien, C.; Mauger, A.; Zaghib, K.; Groult, H. Comparative Issues of Cathode Materials for Li-Ion Batteries. *Inorganics* **2014**, *2* (1), 132–154. <https://doi.org/10.3390/inorganics2010132>.
- (3) Tarascon, J.-M.; Armand, M. *Issues and Challenges Facing Rechargeable Lithium Batteries*; 2001.
- (4) Myung, S. T.; Maglia, F.; Park, K. J.; Yoon, C. S.; Lamp, P.; Kim, S. J.; Sun, Y. K. Nickel-Rich Layered Cathode Materials for Automotive Lithium-Ion Batteries: Achievements and Perspectives. *ACS Energy Letters*. American Chemical Society January 13, 2017, pp 196–223. <https://doi.org/10.1021/acseenergylett.6b00594>.
- (5) Andre, D.; Kim, S. J.; Lamp, P.; Lux, S. F.; Maglia, F.; Paschos, O.; Stiaszny, B. Future Generations of Cathode Materials: An Automotive Industry Perspective. *Journal of Materials Chemistry A*. Royal Society of Chemistry April 7, 2015, pp 6709–6732. <https://doi.org/10.1039/c5ta00361j>.
- (6) Obrovac, M. N.; Chevrier, V. L. Alloy Negative Electrodes for Li-Ion Batteries. *Chemical Reviews*. American Chemical Society December 10, 2014, pp 11444–11502. <https://doi.org/10.1021/cr500207g>.
- (7) Marinaro, M.; Yoon, D. hwan; Gabrielli, G.; Stegmaier, P.; Figgemeier, E.; Spurk, P. C.; Nelis, D.; Schmidt, G.; Chauveau, J.; Axmann, P.; Wohlfahrt-Mehrens, M. High Performance 1.2 Ah Si-Alloy/Graphite|LiNi_{0.5}Mn_{0.3}Co_{0.2}O₂ Prototype Li-Ion Battery. *J. Power Sources* **2017**, *357*, 188–197. <https://doi.org/10.1016/j.jpowsour.2017.05.010>.
- (8) Gabrielli, G.; Marinaro, M.; Mancini, M.; Axmann, P.; Wohlfahrt-Mehrens, M. A New

- Approach for Compensating the Irreversible Capacity Loss of High-Energy Si/C|LiNi_{0.5}Mn_{1.5}O₄ Lithium-Ion Batteries. *J. Power Sources* **2017**, *351*, 35–44. <https://doi.org/10.1016/j.jpowsour.2017.03.051>.
- (9) Yu, X.; Manthiram, A. Sustainable Battery Materials for Next-generation Electrical Energy Storage. *Adv. Energy Sustain. Res.* **2021**, 2000102. <https://doi.org/10.1002/aesr.202000102>.
- (10) IBM Research is reshaping the scene of sustainable batteries <https://www.ibm.com/blogs/nordic-msp/ibm-research-reshaping-scene-of-sustainable-batteries/> (accessed Apr 26, 2021).
- (11) Start - Battery 2030 <https://battery2030.eu/> (accessed Apr 26, 2021).
- (12) Yin, Y. X.; Xin, S.; Guo, Y. G.; Wan, L. J. Lithium-Sulfur Batteries: Electrochemistry, Materials, and Prospects. *Angewandte Chemie - International Edition*. December 9, 2013, pp 13186–13200. <https://doi.org/10.1002/anie.201304762>.
- (13) Peng, H. J.; Huang, J. Q.; Cheng, X. B.; Zhang, Q. Review on High-loading and High-energy Lithium–Sulfur Batteries. *Adv. Energy Mater.* **2017**, *7* (24), 1700260. <https://doi.org/10.1002/aenm.201700260>.
- (14) Fang, R.; Zhao, S.; Sun, Z.; Wang, D. W.; Cheng, H. M.; Li, F. More Reliable Lithium-sulfur Batteries: Status, Solutions and Prospects. *Adv. Mater.* **2017**, *29* (48), 1606823. <https://doi.org/10.1002/adma.201606823>.
- (15) Fan, X.; Sun, W.; Meng, F.; Xing, A.; Liu, J. Advanced Chemical Strategies for Lithium–Sulfur Batteries: A Review. *Green Energy and Environment*. KeAi Publishing Communications Ltd. January 1, 2018, pp 2–19. <https://doi.org/10.1016/j.gee.2017.08.002>.
- (16) Liu, T.; Hu, H.; Ding, X.; Yuan, H.; Jin, C.; Nai, J.; Liu, Y.; Wang, Y.; Wan, Y.; Tao, X. 12 Years Roadmap of the Sulfur Cathode for Lithium Sulfur Batteries (2009–2020). *Energy*

- Storage Materials*. Elsevier B.V. September 1, 2020, pp 346–366.
<https://doi.org/10.1016/j.ensm.2020.05.023>.
- (17) Ji, X.; Lee, K. T.; Nazar, L. F. A Highly Ordered Nanostructured Carbon-Sulphur Cathode for Lithium-Sulphur Batteries. *Nat. Mater.* **2009**, *8* (6), 500–506.
<https://doi.org/10.1038/nmat2460>.
- (18) Mohanty, S. P.; Kishore, B.; Nookala, M. Composites of Sulfur-Titania Nanotubes Prepared by a Facile Solution Infiltration Route as Cathode Material in Lithium-Sulfur Battery. *J. Nanosci. Nanotechnol.* **2018**, *18* (10), 6830–6837. <https://doi.org/10.1166/jnn.2018.15453>.
- (19) Zhang, F.-F.; Huang, G.; Wang, X.-X.; Qin, Y.-L.; Du, X.-C.; Yin, D.-M.; Liang, F.; Wang, L.-M. Sulfur-Impregnated Core-Shell Hierarchical Porous Carbon for Lithium-Sulfur Batteries. *Chem. - A Eur. J.* **2014**, *20* (52), 17523–17529.
<https://doi.org/10.1002/chem.201404439>.
- (20) Wang, H.; Yang, Y.; Liang, Y.; Robinson, J. T.; Li, Y.; Jackson, A.; Cui, Y.; Dai, H. Graphene-Wrapped Sulfur Particles as a Rechargeable Lithium-Sulfur Battery Cathode Material with High Capacity and Cycling Stability. *Nano Lett.* **2011**, *11* (7), 2644–2647.
<https://doi.org/10.1021/nl200658a>.
- (21) Zhou, G.; Yin, L. C.; Wang, D. W.; Li, L.; Pei, S.; Gentle, I. R.; Li, F.; Cheng, H. M. Fibrous Hybrid of Graphene and Sulfur Nanocrystals for High-Performance Lithium-Sulfur Batteries. *ACS Nano* **2013**, *7* (6), 5367–5375. <https://doi.org/10.1021/nn401228t>.
- (22) Zhang, S. S. Role of LiNO₃ in Rechargeable Lithium/Sulfur Battery. *Electrochim. Acta* **2012**, *70*, 344–348. <https://doi.org/10.1016/j.electacta.2012.03.081>.
- (23) Zhao, W.; Yi, J.; He, P.; Zhou, H. Solid-State Electrolytes for Lithium-Ion Batteries: Fundamentals, Challenges and Perspectives. *Electrochem. Energy Rev.* **2019**, *2* (4), 574–

605. <https://doi.org/10.1007/s41918-019-00048-0>.
- (24) Zhang, S. Improved Cyclability of Liquid Electrolyte Lithium/Sulfur Batteries by Optimizing Electrolyte/Sulfur Ratio. *Energies* **2012**, *5* (12), 5190–5197. <https://doi.org/10.3390/en5125190>.
- (25) Zhao, X.; Kim, J. K.; Ahn, H. J.; Cho, K. K.; Ahn, J. H. A Ternary Sulfur/Polyaniline/Carbon Composite as Cathode Material for Lithium Sulfur Batteries. *Electrochim. Acta* **2013**, *109*, 145–152. <https://doi.org/10.1016/j.electacta.2013.07.067>.
- (26) Li, W.; Zhang, Q.; Zheng, G.; Seh, Z. W.; Yao, H.; Cui, Y. Understanding the Role of Different Conductive Polymers in Improving the Nanostructured Sulfur Cathode Performance. *Nano Lett.* **2013**, *13* (11), 5534–5540. <https://doi.org/10.1021/nl403130h>.
- (27) Li, J.; Ding, B.; Xu, G.; Hou, L.; Zhang, X.; Yuan, C. Enhanced Cycling Performance and Electrochemical Reversibility of a Novel Sulfur-Impregnated Mesoporous Hollow TiO₂ Sphere Cathode for Advanced Li-S Batteries. *Nanoscale* **2013**, *5* (13), 5743–5746. <https://doi.org/10.1039/c3nr01393f>.
- (28) Lu, S.; Cheng, Y.; Wu, X.; Liu, J. Significantly Improved Long-Cycle Stability in High-Rate Li-S Batteries Enabled by Coaxial Graphene Wrapping over Sulfur-Coated Carbon Nanofibers. *Nano Lett.* **2013**, *13* (6), 2485–2489. <https://doi.org/10.1021/nl400543y>.
- (29) Xin, S.; Guo, Y. G.; Wan, L. J. Nanocarbon Networks for Advanced Rechargeable Lithium Batteries. *Acc. Chem. Res.* **2012**, *45* (10), 1759–1769. <https://doi.org/10.1021/ar300094m>.
- (30) Xin, S.; Gu, L.; Zhao, N. H.; Yin, Y. X.; Zhou, L. J.; Guo, Y. G.; Wan, L. J. Smaller Sulfur Molecules Promise Better Lithium/Sulfur Batteries. *J. Am. Chem. Soc.* **2012**, *134* (45), 18510–18513. <https://doi.org/10.1021/ja308170k>.
- (31) Wang, J.; Wang, W.; Li, H.; Tan, T.; Wang, X.; Zhao, Y. Carbon Nanotubes/SiC Prepared

- by Catalytic Chemical Vapor Deposition as Scaffold for Improved Lithium-Sulfur Batteries. *J. Nanoparticle Res.* **2019**, *21* (6), 1–10. <https://doi.org/10.1007/s11051-019-4540-3>.
- (32) Wan, C.; Wu, W.; Wu, C.; Xu, J.; Guan, L. A Layered Porous ZrO₂/RGO Composite as Sulfur Host for Lithium-Sulfur Batteries. *RSC Adv.* **2015**, *5* (7), 5102–5106. <https://doi.org/10.1039/c4ra12031k>.
- (33) Qu, Q.; Gao, T.; Zheng, H.; Wang, Y.; Li, X.; Li, X.; Chen, J.; Han, Y.; Shao, J.; Zheng, H. Strong Surface-Bound Sulfur in Conductive MoO₂ Matrix for Enhancing Li-S Battery Performance. *Adv. Mater. Interfaces* **2015**, *2* (7). <https://doi.org/10.1002/admi.201500048>.
- (34) Tao, X.; Wan, J.; Liu, C.; Wang, H.; Yao, H.; Zheng, G.; Seh, Z. W.; Cai, Q.; Li, W.; Zhou, G.; Zu, C.; Cui, Y. Balancing Surface Adsorption and Diffusion of Lithium-Polysulfides on Nonconductive Oxides for Lithium-Sulfur Battery Design. *Nat. Commun.* **2016**, *7*. <https://doi.org/10.1038/ncomms11203>.
- (35) Zhao, C.; Shen, C.; Xin, F.; Sun, Z.; Han, W. Prussian Blue-Derived Fe₂O₃/Sulfur Composite Cathode for Lithium-Sulfur Batteries. *Mater. Lett.* **2014**, *137*, 52–55. <https://doi.org/10.1016/j.matlet.2014.08.115>.
- (36) Yan, B.; Li, X.; Bai, Z.; Song, X.; Xiong, D.; Zhao, M.; Li, D.; Lu, S. A Review of Atomic Layer Deposition Providing High Performance Lithium Sulfur Batteries. *Journal of Power Sources*. Elsevier B.V. January 15, 2017, pp 34–48. <https://doi.org/10.1016/j.jpowsour.2016.10.097>.
- (37) Gu, X.; Lai, C. Recent Development of Metal Compound Applications in Lithium-Sulphur Batteries. *Journal of Materials Research*. Cambridge University Press January 15, 2018, pp 16–31. <https://doi.org/10.1557/jmr.2017.282>.

- (38) Kim, H.; Lee, J. T.; Lee, D.-C.; Magasinski, A.; Cho, W.; Yushin, G. Plasma-Enhanced Atomic Layer Deposition of Ultrathin Oxide Coatings for Stabilized Lithium-Sulfur Batteries. *Adv. Energy Mater.* **2013**, *3* (10), 1308–1315. <https://doi.org/10.1002/aenm.201300253>.
- (39) Yu, M.; Yuan, W.; Li, C.; Hong, J. D.; Shi, G. Performance Enhancement of a Graphene-Sulfur Composite as a Lithium-Sulfur Battery Electrode by Coating with an Ultrathin Al₂O₃ Film via Atomic Layer Deposition. *J. Mater. Chem. A* **2014**, *2* (20), 7360–7366. <https://doi.org/10.1039/c4ta00234b>.
- (40) Shkrob, I. A.; Kropf, A. J.; Marin, T. W.; Li, Y.; Poluektov, O. G.; Niklas, J.; Abraham, D. P. Manganese in Graphite Anode and Capacity Fade in Li Ion Batteries. *J. Phys. Chem. C* **2014**, *118* (42), 24335–24348. <https://doi.org/10.1021/jp507833u>.
- (41) Chen, H.; Dong, W.; Ge, J.; Wang, C.; Wu, X.; Lu, W.; Chen, L. Ultrafine Sulfur Nanoparticles in Conducting Polymer Shell as Cathode Materials for High Performance Lithium/Sulfur Batteries. *Sci. Rep.* **2013**, *3* (1), 1–6. <https://doi.org/10.1038/srep01910>.
- (42) Lee, J.; Choi, W. Surface Modification of Sulfur Cathodes with PEDOT:PSS Conducting Polymer in Lithium-Sulfur Batteries. *J. Electrochem. Soc.* **2015**, *162* (6), A935–A939. <https://doi.org/10.1149/2.0651506jes>.
- (43) Wu, F.; Chen, J.; Chen, R.; Wu, S.; Li, L.; Chen, S.; Zhao, T. Sulfur/Polythiophene with a Core/Shell Structure: Synthesis and Electrochemical Properties of the Cathode for Rechargeable Lithium Batteries. *J. Phys. Chem. C* **2011**, *115* (13), 6057–6063. <https://doi.org/10.1021/jp1114724>.
- (44) Wang, Z.; Chen, Y.; Battaglia, V.; Liu, G. Improving the Performance of Lithium-Sulfur Batteries Using Conductive Polymer and Micrometric Sulfur Powder.

- <https://doi.org/10.1557/jmr.2014.85>.
- (45) Seh, Z. W.; Li, W.; Cha, J. J.; Zheng, G.; Yang, Y.; Mcdowell, M. T.; Hsu, P.-C.; Cui, Y. Sulphur TiO₂ Yolk Shell Nanoarchitecture with Internal Void Space for Long-Cycle Lithium Sulphur Batteries. *Nat. Commun.* **2012**, *4* (1), 1–6. <https://doi.org/10.1038/ncomms2327>.
- (46) Zu, C.; Manthiram, A. Hydroxylated Graphene-Sulfur Nanocomposites for High-Rate Lithium-Sulfur Batteries. *Adv. Energy Mater.* **2013**, *3* (8), 1008–1012. <https://doi.org/10.1002/aenm.201201080>.
- (47) Hu, C.; Chen, H.; Shen, Y.; Lu, D.; Zhao, Y.; Lu, A.-H.; Wu, X.; Lu, W.; Chen, L. In Situ Wrapping of the Cathode Material in Lithium-Sulfur Batteries. *Nat. Commun.* **2017**, *8* (1), 1–9. <https://doi.org/10.1038/s41467-017-00656-8>.
- (48) Song, J.; Gordin, M. L.; Xu, T.; Chen, S.; Yu, Z.; Sohn, H.; Lu, J.; Ren, Y.; Duan, Y.; Wang, D. Strong Lithium Polysulfide Chemisorption on Electroactive Sites of Nitrogen-Doped Carbon Composites For High-Performance Lithium-Sulfur Battery Cathodes. *Angew. Chemie* **2015**, *127* (14), 4399–4403. <https://doi.org/10.1002/ange.201411109>.
- (49) Liang, X.; Nazar, L. F. In Situ Reactive Assembly of Scalable Core–Shell Sulfur–MnO₂ Composite Cathodes. *ACS Nano* **2016**, *10* (4), 4192–4198. <https://doi.org/10.1021/acsnano.5b07458>.
- (50) Liang, C.; Dudney, N. J.; Howe, J. Y. Hierarchically Structured Sulfur/Carbon Nanocomposite Material for High-Energy Lithium Battery. *Chem. Mater.* **2009**, *21* (19), 4724–4730. <https://doi.org/10.1021/cm902050j>.
- (51) Li, H.; Sun, M.; Zhang, T.; Fang, Y.; Wang, G. Improving the Performance of PEDOT-PSS Coated Sulfur@activated Porous Graphene Composite Cathodes for Lithium-Sulfur

- Batteries. *J. Mater. Chem. A* **2014**, *2* (43), 18345–18352.
<https://doi.org/10.1039/c4ta03366c>.
- (52) Tao, X.; Zhang, J.; Xia, Y.; Huang, H.; Du, J.; Xiao, H.; Zhang, W.; Gan, Y. Bio-Inspired Fabrication of Carbon Nanotiles for High Performance Cathode of Li-S Batteries. *J. Mater. Chem. A* **2014**, *2* (7), 2290–2296. <https://doi.org/10.1039/c3ta14113f>.
- (53) Abessolo Ondo, D.; Loyer, F.; Chemin, J.-B.; Bulou, S.; Choquet, P.; Boscher, N. D. Atmospheric Plasma Oxidative Polymerization of Ethylene Dioxythiophene (EDOT) for the Large-Scale Preparation of Highly Transparent Conducting Thin Films. *Plasma Process. Polym.* **2018**, *15* (4), 1700172. <https://doi.org/10.1002/ppap.201700172>.
- (54) Rangasamy, V. S.; Vanhulsel, A. Synthesis and Processing of Battery Materials: Giving It the Plasma Touch. *Batter. Supercaps* **2021**. <https://doi.org/10.1002/batt.202000245>.
- (55) Shafique, A.; Rangasamy, V. S.; Vanhulsel, A.; Safari, M.; Van Bael, M. K.; Hardy, A.; Sallard, S. The Impact of Polymeric Binder on the Morphology and Performances of Sulfur Electrodes in Lithium–Sulfur Batteries. *Electrochim. Acta* **2020**, *360*, 136993. <https://doi.org/10.1016/j.electacta.2020.136993>.
- (56) Ozhukil Kollath, V.; Put, S.; Mullens, S.; Vanhulsel, A.; Luyten, J.; Traina, K.; Cloots, R. Atmospheric Pressure Plasma as an Activation Step for Improving Protein Adsorption on Hydroxyapatite Powder. *Plasma Process. Polym.* **2015**, *12* (6), 594–601. <https://doi.org/10.1002/ppap.201400092>.
- (57) Rego, R. J. M., Havermans, D., & Cools, J. J. Atmospheric-Pressure Plasma Jet. US8552335B2, February 6, 2013.
- (58) Put, S.; Bertels, C.; Vanhulsel, A. Atmospheric Pressure Plasma Treatment of Polymeric Powders. *Surf. Coatings Technol.* **2013**, *234*, 76–81.

- <https://doi.org/10.1016/j.surfcoat.2013.02.006>.
- (59) Xu, J.; Wang, K.; Zu, S. Z.; Han, B. H.; Wei, Z. Hierarchical Nanocomposites of Polyaniline Nanowire Arrays on Graphene Oxide Sheets with Synergistic Effect for Energy Storage. *ACS Nano* **2010**, *4* (9), 5019–5026. <https://doi.org/10.1021/nn1006539>.
- (60) Yang, Y.; Yu, G.; Cha, J. J.; Wu, H.; Vosgueritchian, M.; Yao, Y.; Bao, Z.; Cui, Y. Improving the Performance of Lithium-Sulfur Batteries by Conductive Polymer Coating. *ACS Nano* **2011**, *5* (11), 9187–9193. <https://doi.org/10.1021/nn203436j>.
- (61) Garreau, S.; Louam, G.; Lefrant, S.; Buisson, J. P.; Froyer, G. Optical Study and Vibrational Analysis of the Poly(3,4-Ethylenedioxythiophene) (PEDT). *Synth. Met.* **1999**, *101* (1), 312–313. [https://doi.org/10.1016/S0379-6779\(98\)01146-1](https://doi.org/10.1016/S0379-6779(98)01146-1).
- (62) Lisowska-Oleksiak, A.; Nowak, A. P.; Wilamowska, M.; Sikora, M.; Szczerba, W.; Kapusta, C. Ex Situ XANES, XPS and Raman Studies of Poly(3,4-Ethylenedioxythiophene) Modified by Iron Hexacyanoferrate. *Synth. Met.* **2010**, *160* (11–12), 1234–1240. <https://doi.org/10.1016/j.synthmet.2010.03.015>.
- (63) Chiu, W. W.; Travaš-Sejdić, J.; Cooney, R. P.; Bowmaker, G. A. Studies of Dopant Effects in Poly(3,4-Ethylenedioxythiophene) Using Raman Spectroscopy. *J. Raman Spectrosc.* **2006**, *37* (12), 1354–1361. <https://doi.org/10.1002/jrs.1545>.
- (64) Moraes, B. R.; Campos, N. S.; Izumi, C. M. S. Surface-Enhanced Raman Scattering of EDOT and PEDOT on Silver and Gold Nanoparticles. *Vib. Spectrosc.* **2018**, *96* (January), 137–142. <https://doi.org/10.1016/j.vibspec.2018.04.006>.
- (65) Liu, C.; Goeckner, M. J.; Walker, A. V. Plasma Polymerization of Poly(3,4-Ethylenedioxyethylene) Films: The Influence of Plasma Gas Phase Chemistry. *J. Vac. Sci. Technol. A Vacuum, Surfaces, Film.* **2017**, *35* (2), 021302.

<https://doi.org/10.1116/1.4968017>.

- (66) Zhao, Q.; Jamal, R.; Zhang, L.; Wang, M.; Abdiryim, T. The Structure and Properties of PEDOT Synthesized by Template-Free Solution Method. *Nanoscale Res. Lett.* **2014**, *9* (1), 557. <https://doi.org/10.1186/1556-276X-9-557>.
- (67) Cho, M. S.; Yun, Y. Y.; Nam, J. D.; Son, Y.; Lee, Y. Effect of Magnetic Field on Electrochemical Polymerization of EDOT. *Synth. Met.* **2008**, *158* (21–24), 1043–1046. <https://doi.org/10.1016/j.synthmet.2008.07.006>.
- (68) Ouyang, J.; Xu, Q.; Chu, C. W.; Yang, Y.; Li, G.; Shinar, J. On the Mechanism of Conductivity Enhancement in Poly(3,4- Ethylenedioxythiophene):Poly(Styrene Sulfonate) Film through Solvent Treatment. *Polymer (Guildf)*. **2004**, *45* (25), 8443–8450. <https://doi.org/10.1016/j.polymer.2004.10.001>.
- (69) Megherbi, A.; Meghabar, R.; Belbachir, M. Preparation and Characterization of Clay (Maghnite-H)/Poly(3,4-Ethylenedioxythiophene) Composites. *J. Surf. Eng. Mater. Adv. Technol.* **2013**, *03* (01), 21–27. <https://doi.org/10.4236/jsemat.2013.31004>.
- (70) Zhu, J.; Zhu, P.; Yan, C.; Dong, X.; Zhang, X. Recent Progress in Polymer Materials for Advanced Lithium-Sulfur Batteries. *Progress in Polymer Science*. Elsevier Ltd March 1, 2019, pp 118–163. <https://doi.org/10.1016/j.progpolymsci.2018.12.002>.
- (71) Raulo, A.; Bandyopadhyay, S.; Ahamad, S.; Gupta, A. Bio-Inspired Poly(3,4-Ethylenedioxythiophene): Poly(Styrene Sulfonate)-Sulfur@polyacrylonitrile Electrospun Nanofibers for Lithium-Sulfur Batteries. *J. Power Sources* **2019**, *431* (April), 250–258. <https://doi.org/10.1016/j.jpowsour.2019.05.055>.
- (72) Ahn, S.; Noguchi, T.; Momma, T.; Nara, H.; Yokoshima, T.; Togasaki, N.; Osaka, T. Facile Fabrication of Sulfur/Ketjenblack-PEDOT:PSS Composite as a Cathode with Improved

- Cycling Performance for Lithium Sulfur Batteries. *Chem. Phys. Lett.* **2020**, 749 (February), 137426. <https://doi.org/10.1016/j.cplett.2020.137426>.
- (73) Hong, X.; Liu, Y.; Li, Y.; Wang, X.; Fu, J.; Wang, X. Application Progress of Polyaniline, Polypyrrole and Polythiophene in Lithium-Sulfur Batteries. *Polymers (Basel)*. **2020**, 12 (2). <https://doi.org/10.3390/polym12020331>.
- (74) Chen, H.; Dong, W.; Ge, J.; Wang, C.; Wu, X.; Lu, W.; Chen, L. Ultrafine Sulfur Nanoparticles in Conducting Polymer Shell as Cathode Materials for High Performance Lithium/Sulfur Batteries. *Sci. Rep.* **2013**, 3 (1), 1–6. <https://doi.org/10.1038/srep01910>.
- (75) Dörfler, S.; Althues, H.; Härtel, P.; Abendroth, T.; Schumm, B.; Kaskel, S. Challenges and Key Parameters of Lithium-Sulfur Batteries on Pouch Cell Level. *Joule*. Cell Press March 18, 2020, pp 539–554. <https://doi.org/10.1016/j.joule.2020.02.006>.
- (76) Kang, W.; Deng, N.; Ju, J.; Li, Q.; Wu, D.; Ma, X.; Li, L.; Naebe, M.; Cheng, B. A Review of Recent Developments in Rechargeable Lithium-Sulfur Batteries. *Nanoscale* **2016**, 8 (37), 16541–16588. <https://doi.org/10.1039/c6nr04923k>.
- (77) Sun, K.; Liu, H.; Gan, H. Cathode Loading Effect on Sulfur Utilization in Lithium-Sulfur Battery. *J. Electrochem. Energy Convers. Storage* **2016**, 13 (2). <https://doi.org/10.1115/1.4034738>.
- (78) Xu, J.; Shui, J.; Wang, J.; Wang, M.; Liu, H. K.; Dou, S. X.; Jeon, I. Y.; Seo, J. M.; Baek, J. B.; Dai, L. Sulfur-Graphene Nanostructured Cathodes via Ball-Milling for High-Performance Lithium-Sulfur Batteries. *ACS Nano* **2014**, 8 (10), 10920–10930. <https://doi.org/10.1021/nn5047585>.
- (79) Yuan, L.; Qiu, X.; Chen, L.; Zhu, W. New Insight into the Discharge Process of Sulfur Cathode by Electrochemical Impedance Spectroscopy. *J. Power Sources* **2009**, 189 (1),

127–132. <https://doi.org/10.1016/j.jpowsour.2008.10.033>.

- (80) Deng, Z.; Zhang, Z.; Liu, Y. Electrochemical Impedance Spectroscopy Study of a Lithium/Sulfur Battery: Modeling and Analysis of Capacity Fading. *Artic. J. Electrochem. Soc.* **2013**, *160* (4), A553–A558. <https://doi.org/10.1149/2.026304jes>.
- (81) Cañas, N. A.; Hirose, K.; Pascucci, B.; Wagner, N.; Friedrich, K. A.; Hiesgen, R. Investigations of Lithium-Sulfur Batteries Using Electrochemical Impedance Spectroscopy. *Electrochim. Acta* **2013**, *97*, 42–51. <https://doi.org/10.1016/j.electacta.2013.02.101>.

TOC graphic

